Interferon Regulatory Factor 7 impairs cellular metabolism with age in adipose-derived stromal cells

Alice Nodari[1*], Ilaria Scambi[1*], Daniele Peroni[2*], Elisa Calabria[1], Donatella Benati[1], Silvia Mannucci[1], Marcello Manfredi[3, 8], Andrea Frontini[4], Silvia Visonà[5], Andrea Bozzato[6], Andrea Sbarbati[1], Federico Schena[1], Emilio Marengo[3, 8], Mauro Krampera[7], Mirco Galiè[1]

[1]Dept. Neuroscience, Biomedicine and Movement, Sec. Anatomy and Histology, University of Verona, Verona, Italy
[2]Dept of Cellular, Computational and Integrative Biology, University of Trento, Trento, Italy
[3]Dept of Sciences and Technological Innovation,University of Piemonte Orientale, Alessandria, Italy
[4] Department of Life and Environmental Sciences, Polytechnic University of Marche, Ancona, Italy
[5]Dept of Public Health Experiental and Forensic Medicine, University of Pavia
[6]Dept of Biomedical Sciences and Biotechnology, University of Brescia, Brescia, Italy
[7]Dept of Medicine, Sec. Hematology, Stem Cell Research Laboratory, University of Verona, Italy
[8]Center for Translational Research on Autoimmune and Allergic Disease - CAAD, University of Piemonte Orientale, Novara, Italy

Summary statement

Authors show that the expression of a crucial mediator of the innate immunity, namely Interferon Regulatory Factor 7 (IRF7), increases at cell-autonomous level over the adult life and its increase is mechanistically correlated to aging-like metabolic alterations, such as impaired mitochondrial fitness, reduced amino acid biogenesis and diminished expression of genes involved branched chain amino acid degradation.

Key words:
Aging
IFN signaling
Interferon Regulatory factor 7
Cellular metabolism
Mitochondria
Branched chain amino acid degradation

Correspondence to:
Mirco Galiè, PhD, [1]Dept. Neuroscience, Biomedicine and Movement – Sec. Anatomy and HIstology**,** University of Verona, Via Le Grazie 8, 37134 Verona**,** Italy**,** Phone: +39.045.8027681 - Fax: +39.045.8027163**,** e-mail: mirco.galie@univr.it

*These authors contributed equally

AUTHOR CONTRIBUTIONS

Conceptualization, M.G.; Investigation, M.G., A.N., I.S., D.P., S.M., D.B., M.K., A.F., S.V. E.C., M.M., E.C.; Writing – Original Draft, M.G.; Writing – Review & Editing, M.G., A.F., A.N., D.P., A.S., M.K., S.V.; Funding Acquisition, M.G., A.S., M.K.; Data Curation, M.G., A.N., M.K., S.B., A.F., E.M., F.S., M.M., E.C.; Supervision, M.G.

ACKNOWLEDGMENTS

This work was supported by “Italian Government - Ministero dell’Istruzione, dell’Università e Della Ricerca Scientifica”.

Abstract

Dysregulated immunity and widespread metabolic dysfunctions are the most relevant hallmarks of the passing time over the adult life and their combination at midlife is strongly related to increased vulnerability to diseases. However, their causal connection remains largely unclear. Combining multi-omics and functional analyses on adipose derived stromal cells established from young (1 month) and midlife (12 months) mice we show that the increase of Interferon Regulatory Factor 7 (IRF7) over the adult life drives major metabolic changes, which includes impaired mitochondrial function, altered amino acid biogenesis and reduced expression of genes involved in branched chain amino acid (BCAA) degradation. Our results draw a new paradigm of aging as the 'sterile' activation of a cell-autonomous pathway of self-defense and identify a crucial mediator of this pathway, IRF7, as driver of metabolic dysfunction with age.

Introduction

Competition for food and response to infections are the major challenges for survival and evolution(Darwin, 1859; Fumagalli et al., 2011). To face these challenges, organisms have evolved complex strategies of metabolic adaptation and immunity. Their dysregulation (López-Otín et al., 2016) (Franceschi et al., 2018b) is the major hallmark of the passing time over the adult life and drastically increases vulnerability to diseases by midlife (midlife switch)(Berry et al., 2017; D'Antona et al., 2010; Manaye et al., 2013; Mori et al., 2012; Mori et al., 2014; Rogers et al., 2012; Schaum et al., 2020; Shoji et al., 2016; Timmons et al., 2019; Wu et al., 2014). Nevertheless, the mechanistic connection between metabolic and immune dysfunction with age is still largely unexplored. Some metabolic factors have been proposed which might sustain chronic inflammation with age (excess of nutrients, mitochondrial debris, misfolded/misplaced proteins), but very little is known about whether and how immune effectors might impact on metabolic homeostasis (Franceschi et al., 2018b).

Beside systemic immunity, all nucleated cells are endowed with a cell-autonomous, anciently conserved mechanism of self-defense to counteract microbial infection (MacMicking, 2012; Randow et al., 2013). This works as the first barrier against intruders and may eventually prime systemic response. Type I interferons (IFN I) are the major effectors of cell-autonomous immunity (MacMicking, 2012). The 9 member of the Interferon Regulatory Factors (IRFs) family of transcription factors (named IRF1 to 9) coordinate IFN I activation and function (Honda and Taniguchi, 2006). Along with IRF3, IRF7 is the master activator of type I IFN (Honda et al., 2005) and interact with other transcription factors (STATs, ATF-2, NFkB, CREB, AP-1) to modulate grading and diversification of IFN I -mediated response(Levy et al., 2002; Wathelet et al., 1998). Type I IFN network reprograms the expression of thousands of *interferon stimulated genes (ISG)* (Schneider et al., 2014;

Schoggins et al., 2011), the impact of which is largely unexplored on the biology of non-immune cells (Levy et al., 2002; Wathelet et al., 1998).

We show herein that IRF7 increases with chronological age in adipose-derived stromal cells and drives impairment of mitochondrial function, amino acid biogenesis and branched chain amino acid (BCAA) degradation. Our results identify IRF7 as major causal link between immune and metabolic dysfunctions with age and draw a new paradigm of aging as the 'sterile' (i.e. in absence of viral infection) activation of a cell-autonomous pathway of self-defense which impairs metabolic homeostasis and function in a cell-autonomous fashion.

Results

Age repatterns transcription of IFN-, mitochondrial- and amino acid- related genes.

Previous studies have shown that most age-related metabolic and neurodegenerative dysfunctions occur within the first half of life (12 months of age) in rodents (Berry et al., 2017; D'Antona et al., 2010; Manaye et al., 2013; Mori et al., 2012; Mori et al., 2014; Rogers et al., 2012; Schaum et al., 2020; Shoji et al., 2016; Timmons et al., 2019). Adipose tissue is the central hub of metabolic (Rosen and Spiegelman, 2006) and immune regulation (Wu et al., 2007) and represents an early sensor of the passing time as changes of its transcriptome precede those of other organs over the adult life (Schaum et al., 2020). In a search for cell-intrinsic determinants of homeostatic alterations at middle-age, we performed a whole-genome transcriptional profiling of adipose-derived mesenchymal stromal cells explanted from 1-month-old (1mo; n=3) and 12-month-old (12mo; n=3) mice. To identify functional categories of genes which changed in a coordinated manner, we applied a Gene Set

Enrichment Analysis (GSEA) approach (Subramanian et al., 2005) with a pre-compiled collection of genes belonging to REACTOME functional annotation sets (Fabregat et al., 2016; Milacic et al., 2012; Vastrik et al., 2007) (**Fig 1A**). Cytokine and IFN signaling pathways were the most enriched functional categories in 12-month-old MSCs, while gene associated with respiratory electron transport had the highest enrichment scores (ES) in 1-month-old MSCs (**Fig 1B**). GSEA of mitochondrial-related Gene Ontology (GO) (Ashburner et al., 2000; The Gene Ontology Consortium, 2017) showed the significant enrichment of a large repertoire of mitochondrial genes encoding for structural and functional components, including mitochondrial matrix, ribonucleoproteins, aminoacyl-tRNA synthetases and regulators of the mitochondrial biogenesis in addition to components of the respiratory chain (**Fig 1C, left**). Quantitative PCR analysis confirmed the over-expression of multiple oxidative phosphorylation (OXPHOS) genes in a larger cohort of freshly isolated MSC (**Fig 1C, right**). Consistent with increased mitochondrial gene expression, 1-month-old MSCs showed a higher number of mitochondria. In addition, the organelles displayed larger size and more structured cristae than in 12-month-old MSCs (**Fig 1D**). Analysis of mitochondrial respiration and function indicated quantitative and qualitative differences between 1-month-old and 12-month-old MSCs (Fig 1E). Oxidative function is overall reduced in 12-months MSCs (12mo) compared to 1-month MSCs (1mo) (two-way ANOVA P=0.03). Among the different respiratory states analyzed, oxygen consumption in the uncoupled maximal capacity of mitochondria (ET) is 34% lower in 12mo MCSs compared to 1mo cells (p=0.01) (Fig 1E, I and II). Beside these quantitative data also qualitative analysis revealed further differences in mitochondrial function among the two groups of MSCs. Indeed, data of respiratory states expressed relatively to the maximal ET capacity (Flux Control Ratios – FCR) indicate that, while no difference is found at baseline unstimulated ROUTINE state (Fig 1E, III), in 12-months MSCs cells the fraction of oxygen consumption recorded in the unstimulated dissipative LEAK state is higher compared to the 1-month cells (+56%, P=0.03) (Fig 1E, IV).

Consistently, the net ROUTINE capacity (R-L), determined by physiological substrates uptake and cellular energy requirements, is higher in 1mo cells (+69%, P=0.02). Also, the ET coupling efficiency, accounting for the matching between oxygen consumption and ATP production, is lower in the 12mo MSCs compared to the 1mo MSCs (-4,2%, P=0.03) (Fig 1E, V). These results indicate aging affects mitochondrial respiratory efficiency and lead to increased proton dissipation of mitochondrial inner membrane.

Mitochondrial-related GO terms mentioned above (GO_MITOCHONDRIAL MATRIX, GO_MITOCHONDRIAL_PART, GO_RESPIRATORY-CHAIN, **Fig 1C, left**) comprised 971 unique transcripts (**Fig 1F**). Interestingly, among them, 691 (71%) were identified as IFN targets by the INTERFEROME database, a web-based repository of experimentally verified interferon stimulated genes (ISGs) (Rusinova et al., 2013). This subset of mitochondrial genes was strongly enriched in 1-month-old vs 12-months-old MSCs (**Fig 1G**). Strikingly, the leading-edge subset, i.e. the genes that contributed the most to ES, comprised 221 genes mainly related to amino acid biosynthesis and branched chain amino acid (BCAA) (**Fig 1H**). This suggests that the age-induced changes of IFN signature might be the driving force of a multifaced transcriptional reprogramming which impairs mitochondrial function and alters amino acid metabolism.

Age impairs amino acid metabolism

In line with transcriptomic data, a comparison of the untargeted metabolomic profiles of 1-month-old and 12-months-old MSC (**Fig 2**) revealed a striking depletion of amino acids at middle age (**Fig 2A**). Most of key enzymes involved in amino acid biosynthesis were upregulated at the transcriptional level in 1-month-old compared with 12-months-old MSCs, especially those related to the serine and glycine biosynthesis (**Fig 2B**). The list includes *Asparagine synthetase* (*Asns)*, an established read-out of the activation of *Atf4*, which is the

common transcriptional effector downstream stress response pathways and the master regulator of the amino acid biosynthesis-related genes (Harding et al., 2003).

Genes implicated in the amino acid biosynthesis were identified as ISG according to the INTERFEROME database (**Fig S1A**). Specifically, these genes displayed motifs of varied transcription factors activated by IFN type I and II regulators (**Fig S1B**).

Aside from the transcriptional repression of genes implicated in amino acid biosynthesis, we assessed the expression of genes implicated in amino acid degradation pathways. Most of them were very low expressed, although displayed a slight upregulation with age (**Fig 2C**). In sharp contrast, *Branched chain amino acid transaminase* (*Bcat1* and *2*) displayed a higher expression and were downregulated with age. *Bcat* genes encode for two enzymes which catalyze the first step of the degradation of the branched chain amino acids (BCAA: valine, leucine and isoleucine) (Fig 2D) and yields glutamate as a byproduct. Hence, BCAT are simultaneously implicated in amino acid degradation (BCAA) and synthesis (glutamate). According to INTERFEROME database, the transcriptional changes in AA related genes with age is consistent with the effects of the IFN treatment (**Fig S1C**). To assess more robustly these transcriptional changes in AA metabolic pathways, we executed a qPCR analysis on a higher number of biological replicates of differently aged MSC (1mo MSC cells, n=8; 12mo MSC cells, n=6) (Fig 2E). Although only Bcat1 and Psat1 reached the statistical power, we confirmed a coordinated downregulation with age of BCAA degradation- and AA biosynthesis- related genes and the upregulation of AA degradation-related genes. However, we were not able to detect Ido1 in our qPCR setting.

In silico analyses confirmed the downregulation of mitchondial and BCAA degradation-related genes with age

To further clarify these findings, we interrogated a recently published resource of single-cell transcriptomic data from 3-, 18- and 24-months old mice(Consortium, 2020) (**Fig 2F**).

Specifically, we assessed the expression of genes related to mitochondria structure and function (the 971 genes indicated in Fig 1F), AA biosynthesis (those listed in Fig 2B), AA degradation (those listed in Fig 2C) and BCAA degradation (KEGG mmu00280), on different depots of adipose tissue (brown, BAT, gonadal, GAT, mesenteric, MAT and subcutaneous, SCAT) ether as average of all cell types or as individual values of single resident mesenchymal stem cells (MSC), both in male and female animals. At least in males, we confirmed a strong anti-correlative relation with age of mitochondria-, BCAA degradation- and AA biosynthesis- related genes. Surprisingly, in sharp contrast with our model, also AA degradation related genes displayed a negative correlation, although at a lower extent. Of notice, in line with data from our model, AA degradation genes resulted expressed at very low level. Ido1, in particular was undetectable.

Taken together these findings suggest that while the effect of age on the expression AA degradation-related genes might be variable and context-dependent, the downregulation of of mitchondria, AA biosynthesis and BCAA degradation-related gene is inherently associated to the passing time in males.

IRF7 expression increases with age in multiple organ/tissues

In a search for molecular determinants underlying the transcriptional/metabolic derangement described above, we interrogated our microarray dataset (1mo vs 12mo MSC, n=3 each) for the enrichment of gene sets comprising the targets of 615 different transcription factors (GSEA c3.tft). The most highly enriched gene sets were related to the targets of Interferon Regulatory Factor (IRF) family of transcription factors (**Fig 3A**). Among the nine known members of the IRF family, the only ones readily up-regulated in 12-month-old compared to 1-month-old MSCs were IRF7 and, to a lesser extent, IRF9 (**Fig 3B**). This is in line with the STRING database (Szklarczyk et al., 2017) which reports IRF7 and IRF9 to display the highest frequency of co-expression (**Fig 3C**). We confirmed a remarkable up-

regulation of IRF7 mRNA and protein (**Fig 3D**) in 12-month-old compared to 1-month-old MSCs. Previously identified IRF7-specific targets (Puthia et al., 2016) were also significantly enriched in older MSCs (**Fig 3E**).

The increase of IRF7 with age is not restricted to MSC since we found IRF7 protein to be up-regulated in skeletal muscle (both gastrocnemius and quadriceps), adipose tissue and lungs (but not the spinal cord) of 8-months old mice (n=3) compared to 1-month old mice (n=3) (**Fig 3F, upper panels**). qPCR analysis confirmed the downregulation of mitochondria-, AA biosynthesis- and BCAA degradation- related genes in 8mo adipose tissue and lung, while AA degradation-related genes, such as Got1 and Ido1, were upregulated or unchanged (**Fig 3F, lower panels**).

To further support our findings, we assessed the transcriptional change of IRF7 and its correlation with metabolic genes on a recently published dataset which comprises RNA-seq profiling of multiple organs (gastrocnemious, kidney, liver, hippocampus) from differently aged (6, 9, 12, 18, 21, 24, 27 months) rats(Shavlakadze et al., 2019) (**Fig 3G**). Once again, the analysis confirmed the up-regulation of IRF7 with age, and its inverse correlation with mitochondria- and BCAA-related genes in different organs (gastrocnemious, kidney and liver, but not in hippocampus), while how age correlates with AA biosynthesis- and degradation-associated genes results more controversial.

In addition, we surveyed the expression of IRF7 transcripts across additional publicly available datasets from Gene Expression Ominibus (GEO) databases (**Fig S2**) and confirmed its upregulation at either middle or old age in most tissues/organs (skeletal muscle, adipocytes, heart, kidney, brain, lung) across multiple species. We then interrogated the same GEO datasets for the enrichment of gene sets related to mitochondrial biogenesis and function, translation and amino acid metabolism (**Fig 3H**). In line with the data from MSCs, younger samples across the GEO datasets displayed a strong enrichment of genes related to mitochondrial components, mitochondrial translation machinery and, to a lesser

extent, aminoacyl-tRNA-biosynthesis. Conversely, older samples displayed an enrichment of genes related to the amino acid deprivation. Collectively, these data suggest that IRF7 increases with age in multiple tissue across different species and correlates with the downregulation of mitochondria- and BCAA degradation-related genes.

IRF7 knock down reverts IFN signaling and restores mitochondrial biogenesis

The above data points to IRF7 as the causal connection of the increased interferon signaling and dysregulated cellular metabolism over adult life. To definitively test this hypothesis, we knocked-down IRF7 in 12-month-old MSCs (**Fig 4A**) and executed a new whole-genome microarray profiling. Genes that were significantly (t-test, $p < 0.05$) down-regulated in shIRF7 MSC (12-month-old-shIRF7) were enriched in functional categories related to the antiviral immune response, thus clearly validating the efficiency of the IRF7 loss of function (**Fig 4B and S3)**. On the other hand, genes significantly up-regulated in 12-month-old-shIRF7 were predominantly enriched in mitochondrial and electron transport-related genes (**Fig 4B and S3).** To identify the functional categories of genes that were reversed the most relative to aging, we performed GSEA with the REACTOME collection of gene sets and plotted the ES values of 12-month-old-ctrl vs. shIRF7 against the respective ES value of 1-month-old vs. 12-month-old. Strikingly, interferon signaling pathway and oxidative phosphorylation- related genes sets hit the top up and top down positions, respectively (**Fig 4C**). Also, genes related to “mitochondrial-matrix”, “respiratory chain” and “mitochondrial-part” Gene Ontology categories were significantly enriched in 12-month-old-shIRF7 compared to 12-month-old control cells (**Fig 4D**). According to the transcriptional data, 12mo shIRF7 cells showed a significantly higher number of mitochondria displaying more structured cristae compared to controls (**Fig 4E**).

IRF7 knock-down restores mitochondrial function

To determine whether, besides affecting the expression of mitochondrial gene sets and morphology, IRF7 depletion is relevant also for mitochondrial function, we compared, by using high resolution respirometry (HRR), the rates of oxygen consumption of 12mo shIRF7 versus 12mo ctrl intact cells, in which metabolic responses are essentially based on endogenous substrates (**Fig 5A-C**). A coupling control protocol was used to investigate the different respiratory states (ROUTINE, LEAK and ET). The maximal uncoupled electron transfer capacity (ET) induced by stepwise titration of the uncoupler (CCCP) was significantly increased by 25% (p=0.02) in 12mo-shIRF7 cells compared to controls (**Fig 5A**). Data normalized relatively to ET (Flux Control Ratios, FCR) show that 12mo shIRF7 cells have reduced oxygen consumption in the basal ROUTINE (p=0.004) state as well in the dissipative LEAK state by ≃50% (p=0.02) (**Fig 5B**). Lower oxygen consumption in the ROUTINE and LEAK states is accompanied by an increase of the ET coupling efficiency, expressed as 1-(L/E) (+ 32%; p=0.038) (**Fig 5C**). These results indicate IRF7 knock-down improves mitochondrial respiratory efficiency, probably due to a greater integrity of mitochondrial inner membranes, and thus a reduced proton leak.

IRF7 -induced improvement of OXPHOS function is complex I-linked

To dissect more in depth the impact of IRF7 knock-down on mitochondrial fitness, we permeabilized 12mo shIRF7 and control cells, to allow the entry of specific substrates, and compared their mitochondrial respiration by HRR assays in the ROUTNE, LEAK, OXPHOS and ET respiratory states. To investigate the effects of IRF7 depletion on fatty acids and NADH- dependent pathways we subsequential added octanoylcarnitine fatty acid (FA)/ malate (ETF-linked), malate/glutamate (complex I-linked) and succinate substrates (complex II-linked). These conditions, following ADP stimulation, allow to determine the relative contribution to oxidative phosphorylation (OXPHOS) of β-oxidation, complex-I and

complex-2, respectively. Qualitative analysis of flux control ratios (FCR) allows to evaluate the relative contribution of the various complexes to mitochondrial respiration and highlighted significative qualitative differences in 12mo shIRF7 cells compared to controls. Fatty acids dependent pathways in the OXPHOS state (P_{OM}) are activated at significantly lower levels in 12mo shIRF7 compared to 12mo Ctrl cells (-19%, p=0.02) (**Fig 5D**). In addition investigating the effect of addition of glutamate (G) in the OXPHOS respiratory state, by using the control factor P_{OMG}-P_{OM}/P_{OMG}, we observed a remarkable stimulation in 12mo shIRF7 compared to 12mo ctrl cells (+80%, p=0.02) (**Fig 5E**), suggesting that IRF7 knock-down renders mitochondria more responsive to glutamate stimulation.

IRF7 knock-down partially restores amino acid pool and increases BCAA degradation

The amino acids depleted in 12-month-old cells were all partially restored upon IRF7 knock-down with the exception of the branched chain amino acids (BCAAs) leucine and isoleucine (**Fig 6A**). However, we did not find coordinated changes in the transcription of the genes involved in either amino acid biosynthesis or degradation (**Fig 6B**). This drives us to speculate that the rescue of the amino acid pool after IRF7 knock-down relies on alternative pathways. The fact that, unlike other amino acids, leucine and isoleucine are not restored suggests that IRF7 knock-down allows BCAA degradation pathway to feed into TCA cycle (anaplerosis) to sustain an accelerated flux of intermediates (oxalacetate) for amino acid biosynthesis (**Fig 6C**). In line with this model, genes involved in BCAA degradation are drastically enriched in 12-month-old shIRF7 compared to control (**Fig 6D**). Remarkably, we found a significant upregulation of the gene encoding for PP2Cm (*Ppm1K)*, the mitochondrial localized enzyme which activates the branched-chain, alpha-ketoacid dehydrogenase (BCKDH) complex, the rate-limiting enzyme of the BCAA degradation pathway, and the loss of which has been reported to impair mitochondrial function, increase oxidative stress, and promote abnormal cardiac and neural development (Lu et al., 2007;

Lu et al., 2009). We also found increased transcriptional levels of the Krupple-like factor 15 (*Klf15*) (**Fig 6D**), which has been previously shown to be a master inducer of BCAA degradation genes and crucial to prevent mitochondrial dysfunction and oxidative stress in heart (Gray et al., 2007; Sun et al., 2016a; Sun et al., 2016b). Also, IRF7 knock down completely cleared the aged-induced mehylmaleic acid (citraconic acid), which is an by-product and established diagnostic biomarker of deranged isoleucine degradation which (Duran et al., 1978) **(Fig 6E)**. BCAA degradation may feed TCA cycle by providing succinyl-CoA through which is converted to succinate by *Succinate CoA-ligase GDP forming beta-subunit* (*SuclG2*). Accordingly, succinate was more abundant in 12mo shIRF7 compared to ctrl and *SuclG2* was significantly upregulated (*p = 0.03*) **(Fig 6E)**. Oxalacetate did not accumulate in 12mo shIRF7 cells compared to ctrl, despite the enzyme which generate it from malate, *malate dehydrogenase 1* (*Mdh1*), was markedly upregulated (*p = 0.07*) in shIRF7 cells, while the enzyme which converts oxalacetate to citrate (*Cs*) was downregulated **(Fig 6E)**. This suggests that the rate of oxalacetate generation equals the rate of its cataplerotic diversion toward extra-TCA cycle pathways. Accordingly, the cytoplasmic and mitochondrial isoforms of the enzymes that convert oxalacetate to aspartate (glutamic-oxalacetic transaminase 1 and 2, GOT1 and 2, respectively) are slightly but co-ordinately up-regulated upon shIRF7 cells. Finally, the vast majority of the enzymes involved in the TCA cycle were upregulated in 12mo shIRF7 cells (paired t-test p 0.06), which supports an increased TCA cycle rate (**Fig 6C**).

Confirming that IRF7 knock-down could actually drive the increase in TCA cycle rate, INTERFEROME analysis revealed that all of the TCA cycle genes that had been upregulated in 12-month-old shIRF7 are ISGs and might be regulated upon IFN treatment (**Fig S4A and B**). The same applies for genes involved in the BCAA degradation (**Fig S4C and D**).

IRF7 impairs "core" longevity pathways

Collectively, our data indicate that aging induces the sterile activation of IRF7-mediated metabolic programming, impairing mitochondrial and amino acid biogenesis **(Fig S5)**. Since viruses rely on the bioenergetic and biosynthetic machinery of the host for their replication(Walsh and Mohr, 2011), it might be postulated that the IFN signaling counteracts the viral spread by shutting down "core" metabolic pathways of the host and an overwhelming response may lead to severe impairment of cell and organ functions.

Discussion

The detrimental effects of aging manifests early throughout the course of adult life(Berry et al., 2017; D'Antona et al., 2010; López-Otín et al., 2013; Mori et al., 2012; Mori et al., 2014; Rogers et al., 2012; Shoji et al., 2016; Timmons et al., 2019). The molecular determinants of aging have been recently supposed to follow a non-linear progression rate, with a boost at middle-age (midlife switch)(Timmons et al., 2019), which drastically impairs body fitness and increases vulnerability to metabolic, cardiovascular, locomotory and neurodegenerative and many other types of disorders. As such, according to the “geroscience hypothesis”, the discovery of novel therapeutic strategies capable to prevent the general process of aging is a more straightforward challenge than fighting each of specific age-related disorders in single (Franceschi et al., 2018a)..

We show herein that the increased expression of IRF7 with age leads the sterile activation of cell-autonomous pathways of self-defense which impairs crucial metabolic functions, such as mitochondrial and amino acid biogenesis and BCAA degradation. Our results contribute to draw a novel paradigm in cell biology, setting a causal link between cell-autonomous pathways of self-defense and mitochondrial-centered metabolic pathways, such as respiration, AA biosynthesis and BCAA degradation.

IFNs instructs the transcription of thousands of genes (Interferon stimulated genes, ISGs) (MacMicking, 2012; Randow et al., 2013). While the anti-viral effect of some of these genes is partially clear, the effect of their global repatterning on host cell biology is virtually unexplored. Nevertheless, the IFN-mediated response must be finely tuned as its dysregulated activation may turn detrimental (Baruch et al., 2014; Channappanavar et al., 2016; Davidson et al., 2014; Major et al., 2020; Teijaro et al., 2013). Our results drive us to speculate that one of the major aims of the IFN-mediated response is to shut down the bioenergetic and biosynthetic machinery of the host which would be otherwise usurped by the virus for its own replication(Walsh and Mohr, 2011). The cost-benefits ratio for the host is never obvious, but the opportunity for the cell to embark in such a potentially harmful program might be justified when a real microbial attack in on course. What is less clear is why and how age might activate this program in absence of viral infection.

Nevertheless, a generalized shut-down of crucial metabolic functions may help to explain many aspects of the pathophysiology of aging-related disorders. Mitochondrial and amino acid biogenesis are common outcomes of the ancient evolutionary conserved programs referred to as integrated stress response (ISR)(Harding et al., 2003; Pakos-Zebrucka et al., 2016). These pathways act constitutively as quality control mechanisms and are massively invoked to face multiple acute or chronic stress conditions such as nutrient deprivation, oxidative environment, proteotoxic stress, endoplasmic reticulum overload (Harding et al., 2003; Quirós et al., 2017). The moderate stimulation of these pathways is

on the basis of the beneficial effects of mild-stress interventions such as dietary restriction in preventing aging and even prolonging life-span(Zid et al., 2009) (Mazière et al., 1999). Mitochondria are both targets, and master regulators of these stress response programs. Beyond their bioenergetic role, mitochondria have evolved as signaling organelles which instruct nuclear transcription, cytosolic protein translation and metabolic rewiring to coordinate the cellular adaptation to environmental changes (Cardamone et al., 2018; Chandel, 2015; Quirós et al., 2017; Suhm et al., 2018; Wrobel et al., 2015). Hence, maintenance of proper mitochondrial activity is a priority challenge for cells and organs, which should be accomplished over stress-induced adaptive rearrangements (Harding et al., 2003; Pakos-Zebrucka et al., 2016). The observation that mitochondria of 12mo shIRF7 cells show a reduced OXPHOS capacity sustained by fatty acids suggests that these cells may accumulate less oxidant species (ROS), that are generally accumulated during β-oxidation(Mazière et al., 1999). This condition could explain the improved quality of mitochondrial membranes, consistent both with the enhanced coupling efficiency and with improved morphology of mitochondrial membranes. We cannot say at this stage whether the increase in mitochondrial number and function might be the direct effect of IRF7 knock-down or just a consequence of a chain of event which rescue a young-like phenotype. What is clear is that changes in IRF7 and IFN signaling with age might impact on cellular metabolism which involves mitochondria-centered pathways such as cellular respiration, AA biosynthesis and BCAA degradation.

BCAAs degradation has been extensively implicated in aging and aging-related diseases. Specifically, an increased amount of circulating BCAA and related-metabolites is strongly associated with obesity, type 2 diabetes and heart disease (Felig et al., 1969; Newgard et al., 2009) (Huffman et al., 2009; Li et al., 2017; Lynch and Adams, 2014; Turer et al., 2009). On the other hand, increased expression of genes related to BCAA degradation correlates with insulin sensitivity and boosts fatty acid oxidation (Lerin et al., 2016; Papathanassiu et

al., 2017). BCAA supplementation supports cardiac and skeletal muscle mitochondrial biogenesis, prevents oxidative damage, and promotes exercise capacity in middle-aged animals (D'Antona et al., 2010).

Previous studies in recent years have explored the reciprocal causal connections between mitochondria and inflammation, and their possible role in aging. Recent studies have shown that mitochondrial disruption may trigger inflammatory reactions(Garaude et al., 2016; Jin et al., 2014; Zhang et al., 2010), while pro-inflammatory mediators may contribute, in turn, to alter mitochondrial activity(López-Armada et al., 2006). However, mechanisms modelled in these studies implicate the systemic recruitment of immune cells (neutrophils, macrophages)(Franceschi et al., 2017; Jin et al., 2014), circulating pro-inflammatory cytokines (TNF-alpha, IL6, IL1)(López-Armada et al., 2006; van Horssen et al., 2017), cell debris (Zhang et al., 2010) or DNA damaging chemical mediators (ROS, NOS)(Garaude et al., 2016; Kim et al., 2010) and have ultimately contributed to establish the prevailing notion that the aging-related deterioration of tissue function and mitochondrial integrity relies on a complex bi-directional interaction between systemic immunity and tissue resident cells. We provide herein an additional, cell-intrinsic perspective, which envisions the age-related mitochondrial dysfunction of non-immune cells as the consequence of “cell-autonomous” alterations of immunity-related signaling pathways. IRF7 functions as the molecular trigger of these pathways with aging. Whether the increased expression of IRF7 with age is primed by extrinsic or intrinsic factors is not clear. Nevertheless, its impact on the transcription of immune and mitochondrial genes is cell-autonomous, as it persists in cultured cells over multiple passages, and reversible, thus ruling out the involvement of genetic damages eventually induced by ROS and NOS, previously implicated in connecting inflammatory response with mitochondrial integrity. The role of IRF7 as a regulator of immune cell function has been extensively investigated by thousands of studies. In sharp contrast, its expression and function in non-immune cells remains unexplored. Our data demonstrates that the role

of IRF7 extends beyond the protection against external intruders and its gain of function may indeed represent an intrinsic paradigm of the degeneration over the adulthood.

Our results suggest IRF7 as an ideal target for the development of therapies which are potentially effective against multiple and intersecting aspects of aging phenotype.

Materials and Methods

Isolation of Adipose derived MSCs

The inguinal fat pads of FVB male mice aged 1 (n=8) and 12 (n=8) months were surgically excised, weighed and processed to isolate the adipose-derived stromal cells, according to standard protocols (Peroni et al., 2008). Briefly, the extracellular matrix was digested with collagenase (1 mg/ml) and centrifuged to obtain a high-density pellet, the stromal vascular fraction (SVF). After centrifugation, the SVF cell number was determined using light microscopy, and the cells were plated at a concentration of 1×10^5 cells/cm^2 using DMEM medium (with high glucose concentration, GLUTAMAX I™, 10% FCS, 100 U/ml penicillin and 100 µg/ml streptomycin). After 2 to 3 weeks of culture, a homogeneous cell population was obtained. The cells were identified as MSCs on the basis of their immunophenotype. Specifically, the positivity of CD106 (VCAM1), CD73, CD29, CD44, CD90 and the lack of hematopoietic (antiCD45, CD14, CD11c, CD123 and CD34 monoclonal antibodies) and endothelial cell markers (with CD31 monoclonal antibody) were assessed by means of cytofluorimetric analysis. Animals were handled accordingly with the regulations of the Italian Ministry of Health and to the European Communities Council (86/609/EEC) directives.

Microarray Analyses

Whole-genome microarray analysis of MSC from differently aged mice was performed using the NimbleGen Gene Expression system. Briefly, total RNA was isolated from samples using the Qiagen RNeasy kit (Qiagen), following the manufacturer's instructions. RNA was used for cDNA synthesis followed by labeling of the cDNA with Cy3. The labeled cDNA samples were hybridized to *Mus musculus* 12x135K Array (Roche NimbleGen) which represents 44,170 mouse genes. The single color NimbleGen arrays were scanned with GenePix 4400A Microarray Scanner. The data were extracted from scanned images using NimbleScan software and the Robust Multichip Average (RMA) algorithm was used to generate gene expression values. Hybridization, scanning and normalization of the data were performed as service by the Functional Genomic Center of the University of Verona (Verona, Italy). Raw and processed data are available at Gene Expression Omnibus (GEO) repository (https://www.ncbi.nlm.nih.gov/geo/) under the Accession no. GSE25069. Whole-genome microarray of shIRF7 silenced 12months-old MSC was performed as service by the UTSW Genomics Sequencing & Microarray Core Facility (Dallas, Texas, USA) on an Affymetrix platform (Clariom S Mouse Array). Raw and processed data are available at GEO under the Accession no. GSE168533.

Western Blotting

Immunoblots were performed according to standard procedures in RIPA buffer (150 mM NaCl, 10 mM Tris pH 7.5, 1% NP40, 1% Deoxycholate, 0.1% SDS) supplemented with phosphatase and protease inhibitors (SIGMA). Samples were resolved on Tris-glycine 4-20% gradient SDS-PAGE (BIO-RAD), blotted on Protran® membrane 0.2 µm (Whatman), incubated with the anti-IRF7 antibody [EPR4718] (Abcam #ab109255) and developed with ECL (Amersham).

Quantitative PCR

RNA was extracted using the Qiagen RNAeasy Plus mini kit. cDNA was generated by Superscript II (Invitrogen) and used with SYBR Green PCR master mix (Applied Biosystems) for real-time qPCR analysis. Assays were performed using an Applied Biosystems Step-One Real-Time PCR System. Primers used for qPCR amplification are detailed in Table 1.

Transmission electron microscopy

Samples were fixed with glutaraldehyde 2% in a Sorensen buffer pH 7.4 for 2 h, post-fixed in 1% osmium tetroxide in an aqueous solution for 2 h, dehydrated in graded concentrations of acetone, embedded in Epon-Araldite and cut with an Ultracut E Ultra-microtome (Reichert, Wien, Austria). At the end of the dehydrating process, samples were positioned in a multi-well grid for electron microscopy and observed using a TEM Morgagni 268D (FEI Philips). Quantification of mitochondrial size was performed using ImageJ software on the images taken at the same magnification from 20 randomly selected fields.

shRNA IRF7 lentiviral transduction

IRF7 was silenced in 12mo aged MSC by lentiviral transduction. 4 different shIRF7 into pLKO.1 vectors were used, named #1 (Dharmacon RMM3981-201795252), #2 (Dharmacon RMM3981-201798737), #3 (Dharmacon RMM3981-201788865) and #4 (Dharmacon RMM3981-201789942). Recombinant lentiviruses were generated in 293T cells transfected using the second-generation packaging vectors psPAX2 (Addgene#12260) and pMD2.G (Addgene#12259) using Lentifectin transfection reagent (ABM Good). Stably shIRF7 cells were selected with 1mg/mL Puromycin. 12mo MSC transduced with Empty (Addgene#10878) and shRNA scramble pLKO.1 (Addgene#1864) vectors were used as controls.

Metabolomic Analysis

Cells were trypsinized, washed with PBS solution and centrifuged. Supernatants were removed, and cells were resuspended in PBS. Aliquots containing $1x10^6$ of cells were used for the metabolite extraction. Metabolites were extracted using 760 µL of a precooled MeOH-Water mixture (1:0.9, v/v). Extracts were vortexed until complete dissolution of the pellet and 400 µL of ice-cold chloroform were added. Cells extracts were then homogenized with cell disrupter at 30 Hz for 10 min and centrifuged at 2200 g for 5 min at 4 °C. After layer separation, the polar and the nonpolar fractions were transferred to new precooled tubes. The aliquots were then evaporated to dryness using a nitrogen flow and stored at 80 °C until analysis. Hexadecanoic acid as internal standard was added to the dried extract: the samples were first oximated by adding 30 µL of methoxyamine hydrochloride solution in pyridine (20 mg/mL), mixed in a vortex mixer and subsequently shaken for 90 min at 30 °C. Afterward, 30 µL of N,O-Bis(trimetylsilyl)trifluoroacetamide (BSTFA) with 1% trimethylchlorosilane (TMCS) were added and the derivatization was performed at 70 °C for 60 minutes prior to GC-MS analysis. An alkane standard mixture (C8-C20) was added as internal standard.

Gas chromatography–time of flight mass spectrometry (GC-TOF/MS) was performed using the Agilent 7890B GC (Agilent Technologies, USA) and Pegasus (BT) TOF-MS system (Leco Corporation, USA) equipped with an Rxi–5ms column (30m×0.25mm×0.25µm, RESTEK, USA), stationary phase 5% diphenyl-95% dimethyl polysiloxane. High-purity helium (99.999%) was used as the carrier gas at a flow rate of 1.20 mL/min^{-1}. Samples were injected in splitless mode at 250°C. The chromatographic conditions were: initial temperature 70°C, 2-minute isothermal, 6°C/min up to 160°C, 10°C/min up to 240°C, 20°C/min up to 300°C, 6 minutes isothermal. MS parameters: electron impact ionization source temperature (EI, 70 eV) was set at 250°C; scan range 40/630 m/z, with an extraction frequency of 30 kHz. The chromatograms were acquired in TIC (total ion current) mode.

Mass spectral assignment was performed using the ChromaTOF BT software (Leco Corporation, USA) by matching with NIST MS Search 2.2. Libraries implemented with the MoNa Fiehns Libraries. Statistical and pathway studies were carried out by MetaboAnalyst 4.0 tool.

Mitochondrial respiration

Mitochondrial respiration

To analyze mitochondrial respiration in MSCs cells (transfercted with Ctrl or shIRF7 vectors) we used an Oxygraph-2K (Oroboros Instruments, Innsbruck). Instrumental and chemical background fluxes were opportunely calibrated as a function of oxygen concentration using DatLab software (Oroboros Instruments, Innsbruck). All the measures were performed comparing 12mo-ctrl and 12mo-shIRF7 cells in parallel in the same experiment. Mitochondrial respiration was evaluated both in intact and permeabilized cells in different respiratory states (ROUTINE, LEAK, OXPHOS and ET) (Calabria et al., 2019) (Erich, 2020).

Intact cells: cells resuspended in DMEM (250.000/ml) were analyzed applying a coupling control protocol (Pesta and Gnaiger, 2012) to determine the rate of oxygen consumption in the various respiratory states: ROUTINE (R), LEAK respiration (L), Electron Transfer capacity (ET) and Residual Oxygen Consumption ROX (Pesta and Gnaiger, 2012). After stabilization of the rate of oxygen consumption in the ROUTINE respiration was supported with addition of pyruvate and malate (5 mM and 2 mM, respectively) (Sigma Aldrich), the ATP-synthase inhibitor oligomycin (Omy, 2 µg/mL) (Sigma Aldrich) was added to obtain a measure of LEAK respiration. To this step followed the titration of CCCP to obtain maximum oxygen flux (ET capacity). Finally, Rotenone (Rot) and Antimycin A (Ama) were added to inhibit specifically complex I and III respectively and obtain residual oxygen consumption (ROX).

Permeabilized cells: the respiration of permeabilized cells was determined using a modified substrate-uncoupler-inhibitor titration (SUIT) protocol (Pesta and Gnaiger, 2012). To investigate the contribution of different mitochondrial complexes (I-IV) to respiratory capacity, cells were permeabilized with the mild detergent digitonin (12 µg/10^{-6} cells, Sigma Aldrich), this procedure allows specific substrates and adenylates to enter the cells and reach mitochondria. The optimal concentration of digitonin was evaluated in preliminary experiments as suitable to achieve full permeabilization of cells allowing the access of substrates and ADP to mitochondria without compromising mitochondrial function. To evaluate the contribute of fatty acids to mitochondrial activity Octanoylcarnitine and Malate (OM; 0.8 mM and 2 mM respectively) were added in the ROUTINE state (R_{OM}). Following permeabilization with digitonin, the OXHPOS capacity (P_{OM}) was induced by adding ADP (5mM, Sigma Aldrich) and successively Glutamate (G; 10mM), were used to determine complex I activity (P_{OMG}). To activate also complex II in the OXPHOS, the succinate (P_{OMGS}) was added (10 mM, Sigma Aldrich). The presence of all these substrates (OMGS) allows detecting the respiratory activity of linked complexes I, ETF and complex II. The contribution of complexes III and IV to respiratory activity is always present, although they were not stimulated by the addition of specific substrates.

To analyze the electron transfer system (ET_{OMGS}) capacity, steps titrations with the uncoupler CCCP (0.5 µM steps; Sigma Aldrich) were performed. Rot and Ama (2 and 2.5 µM respectively; Sigma Aldrich) were added to inhibit complex I (ET_S) and III determining residual oxygen consumption (ROX). Raw data were analyzed with DatLab 6 Program (Oroboros Instruments).

Competing interests

No competing interests declared

Data availability

Raw and processed data of the microarray profiling of 1mo vs 12mo MSC are available at Gene Expression Omnibus (GEO) repository (https://www.ncbi.nlm.nih.gov/geo/) under the Accession no. GSE25069. Raw and processed data of the microarray profiling of shIRF7 vs ctrl 12mo MSC are available at GEO under the Accession no. GSE168533.

References

Ashburner, M., Ball, C. A., Blake, J. A., Botstein, D., Butler, H., Cherry, J. M., Davis, A. P., Dolinski, K., Dwight, S. S., Eppig, J. T. et al. (2000). Gene ontology: tool for the unification of biology. The Gene Ontology Consortium. *Nat Genet* **25**, 25-9.

Baruch, K., Deczkowska, A., David, E., Castellano, J. M., Miller, O., Kertser, A., Berkutzki, T., Barnett-Itzhaki, Z., Bezalel, D., Wyss-Coray, T. et al. (2014). Aging. Aging-induced type I interferon response at the choroid plexus negatively affects brain function. *Science* **346**, 89-93.

Berry, D. C., Jiang, Y., Arpke, R. W., Close, E. L., Uchida, A., Reading, D., Berglund, E. D., Kyba, M. and Graff, J. M. (2017). Cellular Aging Contributes to Failure of Cold-Induced Beige Adipocyte Formation in Old Mice and Humans. *Cell Metab* **25**, 166-181.

Calabria, E., Scambi, I., Bonafede, R., Schiaffino, L., Peroni, D., Potrich, V., Capelli, C., Schena, F. and Mariotti, R. (2019). ASCs-Exosomes Recover Coupling Efficiency and Mitochondrial Membrane Potential in an. *Front Neurosci* **13**, 1070.

Cardamone, M. D., Tanasa, B., Cederquist, C. T., Huang, J., Mahdaviani, K., Li, W., Rosenfeld, M. G., Liesa, M. and Perissi, V. (2018). Mitochondrial Retrograde Signaling in Mammals Is Mediated by the Transcriptional Cofactor GPS2 via Direct Mitochondria-to-Nucleus Translocation. *Mol Cell* **69**, 757-772.e7.

Chandel, N. S. (2015). Evolution of Mitochondria as Signaling Organelles. *Cell Metab* **22**, 204-6.

Channappanavar, R., Fehr, A. R., Vijay, R., Mack, M., Zhao, J., Meyerholz, D. K. and Perlman, S. (2016). Dysregulated Type I Interferon and Inflammatory Monocyte-Macrophage Responses Cause Lethal Pneumonia in SARS-CoV-Infected Mice. *Cell Host Microbe* **19**, 181-93.

Consortium, T. M. (2020). A single-cell transcriptomic atlas characterizes ageing tissues in the mouse. *Nature* **583**, 590-595.

D'Antona, G., Ragni, M., Cardile, A., Tedesco, L., Dossena, M., Bruttini, F., Caliaro, F., Corsetti, G., Bottinelli, R., Carruba, M. O. et al. (2010). Branched-chain amino acid supplementation promotes survival and supports cardiac and skeletal muscle mitochondrial biogenesis in middle-aged mice. *Cell Metab* **12**, 362-372.

Darwin, C. (1859). On the origin of species by means of natural selection, or, The preservation of favoured races in the struggle for life: John Murray

Davidson, S., Crotta, S., McCabe, T. M. and Wack, A. (2014). Pathogenic potential of interferon αβ in acute influenza infection. *Nat Commun* **5**, 3864.

Duran, M., Bruinvis, L., Ketting, D. and Wadman, S. K. (1978). Deranged isoleucine metabolism during ketotic attacks in patients with methylmalonic acidaemia. *J Inherit Metab Dis* **1**, 105-7.

Erich, G. (2020). Mitochondrial physiology, vol. 1. Bioenerg Commun.

Fabregat, A., Sidiropoulos, K., Garapati, P., Gillespie, M., Hausmann, K., Haw, R., Jassal, B., Jupe, S., Korninger, F., McKay, S. et al. (2016). The Reactome pathway Knowledgebase. *Nucleic Acids Res* **44**, D481-7.

Felig, P., Marliss, E. and Cahill, G. F. (1969). Plasma amino acid levels and insulin secretion in obesity. *N Engl J Med* **281**, 811-6.

Franceschi, C., Garagnani, P., Morsiani, C., Conte, M., Santoro, A., Grignolio, A., Monti, D., Capri, M. and Salvioli, S. (2018a). The Continuum of Aging and Age-Related Diseases: Common Mechanisms but Different Rates. *Front Med (Lausanne)* **5**, 61.

Franceschi, C., Garagnani, P., Parini, P., Giuliani, C. and Santoro, A. (2018b). Inflammaging: a new immune-metabolic viewpoint for age-related diseases. *Nat Rev Endocrinol* **14**, 576-590.

Franceschi, C., Garagnani, P., Vitale, G., Capri, M. and Salvioli, S. (2017). Inflammaging and 'Garb-aging'. *Trends Endocrinol Metab* **28**, 199-212.

Fumagalli, M., Sironi, M., Pozzoli, U., Ferrer-Admetlla, A., Ferrer-Admettla, A., Pattini, L. and Nielsen, R. (2011). Signatures of environmental genetic adaptation pinpoint pathogens as the main selective pressure through human evolution. *PLoS Genet* **7**, e1002355.

Garaude, J., Acín-Pérez, R., Martínez-Cano, S., Enamorado, M., Ugolini, M., Nistal-Villán, E., Hervás-Stubbs, S., Pelegrín, P., Sander, L. E., Enríquez, J. A. et al. (2016). Mitochondrial respiratory-chain adaptations in macrophages contribute to antibacterial host defense. *Nat Immunol* **17**, 1037-1045.

Gray, S., Wang, B., Orihuela, Y., Hong, E. G., Fisch, S., Haldar, S., Cline, G. W., Kim, J. K., Peroni, O. D., Kahn, B. B. et al. (2007). Regulation of gluconeogenesis by Krüppel-like factor 15. *Cell Metab* **5**, 305-12.

Harding, H. P., Zhang, Y., Zeng, H., Novoa, I., Lu, P. D., Calfon, M., Sadri, N., Yun, C., Popko, B., Paules, R. et al. (2003). An integrated stress response regulates amino acid metabolism and resistance to oxidative stress. *Mol Cell* **11**, 619-33.

Honda, K. and Taniguchi, T. (2006). IRFs: master regulators of signalling by Toll-like receptors and cytosolic pattern-recognition receptors. *Nat Rev Immunol* **6**, 644-58.

Honda, K., Yanai, H., Negishi, H., Asagiri, M., Sato, M., Mizutani, T., Shimada, N., Ohba, Y., Takaoka, A., Yoshida, N. et al. (2005). IRF-7 is the master regulator of type-I interferon-dependent immune responses. *Nature* **434**, 772-7.

Huffman, K. M., Shah, S. H., Stevens, R. D., Bain, J. R., Muehlbauer, M., Slentz, C. A., Tanner, C. J., Kuchibhatla, M., Houmard, J. A., Newgard, C. B. et al. (2009). Relationships between circulating metabolic intermediates and insulin action in overweight to obese, inactive men and women. *Diabetes Care* **32**, 1678-83.

Jin, Z., Wei, W., Yang, M., Du, Y. and Wan, Y. (2014). Mitochondrial complex I activity suppresses inflammation and enhances bone resorption by shifting macrophage-osteoclast polarization. *Cell Metab* **20**, 483-98.

Kim, J., Xu, M., Xo, R., Mates, A., Wilson, G. L., Pearsall, A. W. and Grishko, V. (2010). Mitochondrial DNA damage is involved in apoptosis caused by pro-inflammatory cytokines in human OA chondrocytes. *Osteoarthritis Cartilage* **18**, 424-32.

Lerin, C., Goldfine, A. B., Boes, T., Liu, M., Kasif, S., Dreyfuss, J. M., De Sousa-Coelho, A. L., Daher, G., Manoli, I., Sysol, J. R. et al. (2016). Defects in muscle branched-chain amino acid oxidation contribute to impaired lipid metabolism. *Mol Metab* **5**, 926-936.

Levy, D. E., Marié, I., Smith, E. and Prakash, A. (2002). Enhancement and diversification of IFN induction by IRF-7-mediated positive feedback. *J Interferon Cytokine Res* **22**, 87-93.

Li, T., Zhang, Z., Kolwicz, S. C., Abell, L., Roe, N. D., Kim, M., Zhou, B., Cao, Y., Ritterhoff, J., Gu, H. et al. (2017). Defective Branched-Chain Amino Acid Catabolism Disrupts Glucose Metabolism and Sensitizes the Heart to Ischemia-Reperfusion Injury. *Cell Metab* **25**, 374-385.

Lu, G., Ren, S., Korge, P., Choi, J., Dong, Y., Weiss, J., Koehler, C., Chen, J. N. and Wang, Y. (2007). A novel mitochondrial matrix serine/threonine protein phosphatase regulates the mitochondria permeability transition pore and is essential for cellular survival and development. *Genes Dev* **21**, 784-96.

Lu, G., Sun, H., She, P., Youn, J. Y., Warburton, S., Ping, P., Vondriska, T. M., Cai, H., Lynch, C. J. and Wang, Y. (2009). Protein phosphatase 2Cm is a critical regulator of branched-chain amino acid catabolism in mice and cultured cells. *J Clin Invest* **119**, 1678-87.

Lynch, C. J. and Adams, S. H. (2014). Branched-chain amino acids in metabolic signalling and insulin resistance. *Nat Rev Endocrinol* **10**, 723-36.

López-Armada, M. J., Caramés, B., Martín, M. A., Cillero-Pastor, B., Lires-Dean, M., Fuentes-Boquete, I., Arenas, J. and Blanco, F. J. (2006). Mitochondrial activity is modulated by TNFalpha and IL-1beta in normal human chondrocyte cells. *Osteoarthritis Cartilage* **14**, 1011-22.

López-Otín, C., Blasco, M. A., Partridge, L., Serrano, M. and Kroemer, G. (2013). The hallmarks of aging. *Cell* **153**, 1194-217.

López-Otín, C., Galluzzi, L., Freije, J. M. P., Madeo, F. and Kroemer, G. (2016). Metabolic Control of Longevity. *Cell* **166**, 802-821.

MacMicking, J. D. (2012). Interferon-inducible effector mechanisms in cell-autonomous immunity. *Nat Rev Immunol* **12**, 367-82.

Major, J., Crotta, S., Llorian, M., McCabe, T. M., Gad, H. H., Priestnall, S. L., Hartmann, R. and Wack, A. (2020). Type I and III interferons disrupt lung epithelial repair during recovery from viral infection. *Science*.

Manaye, K. F., Mouton, P. R., Xu, G., Drew, A., Lei, D. L., Sharma, Y., Rebeck, G. W. and Turner, S. (2013). Age-related loss of noradrenergic neurons in the brains of triple transgenic mice. *Age (Dordr)* **35**, 139-47.

Mazière, C., Conte, M. A., Degonville, J., Ali, D. and Mazière, J. C. (1999). Cellular enrichment with polyunsaturated fatty acids induces an oxidative stress and activates the transcription factors AP1 and NFkappaB. *Biochem Biophys Res Commun* **265**, 116-22.

Milacic, M., Haw, R., Rothfels, K., Wu, G., Croft, D., Hermjakob, H., D'Eustachio, P. and Stein, L. (2012). Annotating cancer variants and anti-cancer therapeutics in reactome. *Cancers (Basel)* **4**, 1180-211.

Mori, M. A., Raghavan, P., Thomou, T., Boucher, J., Robida-Stubbs, S., Macotela, Y., Russell, S. J., Kirkland, J. L., Blackwell, T. K. and Kahn, C. R. (2012). Role of microRNA processing in adipose tissue in stress defense and longevity. *Cell Metab* **16**, 336-47.

Mori, M. A., Thomou, T., Boucher, J., Lee, K. Y., Lallukka, S., Kim, J. K., Torriani, M., Yki-Järvinen, H., Grinspoon, S. K., Cypess, A. M. et al. (2014). Altered miRNA processing disrupts brown/white adipocyte determination and associates with lipodystrophy. *J Clin Invest* **124**, 3339-51.

Newgard, C. B., An, J., Bain, J. R., Muehlbauer, M. J., Stevens, R. D., Lien, L. F., Haqq, A. M., Shah, S. H., Arlotto, M., Slentz, C. A. et al. (2009). A branched-chain amino acid-related metabolic signature that differentiates obese and lean humans and contributes to insulin resistance. *Cell Metab* **9**, 311-26.

Pakos-Zebrucka, K., Koryga, I., Mnich, K., Ljujic, M., Samali, A. and Gorman, A. M. (2016). The integrated stress response. *EMBO Rep* **17**, 1374-1395.

Papathanassiu, A. E., Ko, J. H., Imprialou, M., Bagnati, M., Srivastava, P. K., Vu, H. A., Cucchi, D., McAdoo, S. P., Ananieva, E. A., Mauro, C. et al. (2017). BCAT1 controls metabolic reprogramming in activated human macrophages and is associated with inflammatory diseases. *Nat Commun* **8**, 16040.

Peroni, D., Scambi, I., Pasini, A., Lisi, V., Bifari, F., Krampera, M., Rigotti, G., Sbarbati, A. and Galie, M. (2008). Stem molecular signature of adipose-derived stromal cells. *Exp Cell Res* **314**, 603-15.

Pesta, D. and Gnaiger, E. (2012). High-resolution respirometry: OXPHOS protocols for human cells and permeabilized fibers from small biopsies of human muscle. *Methods Mol Biol* **810**, 25-58.

Puthia, M., Ambite, I., Cafaro, C., Butler, D., Huang, Y., Lutay, N., Rydström, G., Gullstrand, B., Swaminathan, B., Nadeem, A. et al. (2016). IRF7 inhibition prevents destructive innate immunity-A target for nonantibiotic therapy of bacterial infections. *Sci Transl Med* **8**, 336ra59.

Quirós, P. M., Prado, M. A., Zamboni, N., D'Amico, D., Williams, R. W., Finley, D., Gygi, S. P. and Auwerx, J. (2017). Multi-omics analysis identifies ATF4 as a key regulator of the mitochondrial stress response in mammals. *J Cell Biol* **216**, 2027-2045.

Randow, F., MacMicking, J. D. and James, L. C. (2013). Cellular self-defense: how cell-autonomous immunity protects against pathogens. *Science* **340**, 701-6.

Rogers, N. H., Landa, A., Park, S. and Smith, R. G. (2012). Aging leads to a programmed loss of brown adipocytes in murine subcutaneous white adipose tissue. *Aging Cell* **11**, 1074-83.

Rosen, E. D. and Spiegelman, B. M. (2006). Adipocytes as regulators of energy balance and glucose homeostasis. *Nature* **444**, 847-53.

Rusinova, I., Forster, S., Yu, S., Kannan, A., Masse, M., Cumming, H., Chapman, R. and Hertzog, P. J. (2013). Interferome v2.0: an updated database of annotated interferon-regulated genes. *Nucleic Acids Res* **41**, D1040-6.

Schaum, N., Lehallier, B., Hahn, O., Pálovics, R., Hosseinzadeh, S., Lee, S. E., Sit, R., Lee, D. P., Losada, P. M., Zardeneta, M. E. et al. (2020). Ageing hallmarks exhibit organ-specific temporal signatures. *Nature* **583**, 596-602.

Schneider, W. M., Chevillotte, M. D. and Rice, C. M. (2014). Interferon-stimulated genes: a complex web of host defenses. *Annu Rev Immunol* **32**, 513-45.

Schoggins, J. W., Wilson, S. J., Panis, M., Murphy, M. Y., Jones, C. T., Bieniasz, P. and Rice, C. M. (2011). A diverse range of gene products are effectors of the type I interferon antiviral response. *Nature* **472**, 481-5.

Shavlakadze, T., Morris, M., Fang, J., Wang, S. X., Zhu, J., Zhou, W., Tse, H. W., Mondragon-Gonzalez, R., Roma, G. and Glass, D. J. (2019). Age-Related Gene Expression Signature in Rats Demonstrate Early, Late, and Linear Transcriptional Changes from Multiple Tissues. *Cell Rep* **28**, 3263-3273.e3.

Shoji, H., Takao, K., Hattori, S. and Miyakawa, T. (2016). Age-related changes in behavior in C57BL/6J mice from young adulthood to middle age. *Mol Brain* **9**, 11.

Subramanian, A., Tamayo, P., Mootha, V. K., Mukherjee, S., Ebert, B. L., Gillette, M. A., Paulovich, A., Pomeroy, S. L., Golub, T. R., Lander, E. S. et al. (2005). Gene set enrichment analysis: a knowledge-based approach for interpreting genome-wide expression profiles. *Proc Natl Acad Sci U S A* **102**, 15545-50.

Suhm, T., Kaimal, J. M., Dawitz, H., Peselj, C., Masser, A. E., Hanzén, S., Ambrožič, M., Smialowska, A., Björck, M. L., Brzezinski, P. et al. (2018). Mitochondrial Translation Efficiency Controls Cytoplasmic Protein Homeostasis. *Cell Metab* **27**, 1309-1322.e6.

Sun, H., Olson, K. C., Gao, C., Prosdocimo, D. A., Zhou, M., Wang, Z., Jeyaraj, D., Youn, J. Y., Ren, S., Liu, Y. et al. (2016a). Catabolic Defect of Branched-Chain Amino Acids Promotes Heart Failure. *Circulation* **133**, 2038-49.

Sun, N., Youle, R. J. and Finkel, T. (2016b). The Mitochondrial Basis of Aging. *Mol Cell* **61**, 654-666.

Szklarczyk, D., Morris, J. H., Cook, H., Kuhn, M., Wyder, S., Simonovic, M., Santos, A., Doncheva, N. T., Roth, A., Bork, P. et al. (2017). The STRING database in 2017: quality-controlled protein-protein association networks, made broadly accessible. *Nucleic Acids Res* **45**, D362-D368.

Teijaro, J. R., Ng, C., Lee, A. M., Sullivan, B. M., Sheehan, K. C., Welch, M., Schreiber, R. D., de la Torre, J. C. and Oldstone, M. B. (2013). Persistent LCMV infection is controlled by blockade of type I interferon signaling. *Science* **340**, 207-11.

The Gene Ontology Consortium. (2017). Expansion of the Gene Ontology knowledgebase and resources. *Nucleic Acids Res* **45**, D331-D338.

Timmons, J. A., Volmar, C. H., Crossland, H., Phillips, B. E., Sood, S., Janczura, K. J., Törmäkangas, T., Kujala, U. M., Kraus, W. E., Atherton, P. J. et al. (2019). Longevity-related molecular pathways are subject to midlife "switch" in humans. *Aging Cell*, e12970.

Turer, A. T., Stevens, R. D., Bain, J. R., Muehlbauer, M. J., van der Westhuizen, J., Mathew, J. P., Schwinn, D. A., Glower, D. D., Newgard, C. B. and Podgoreanu, M. V. (2009). Metabolomic profiling reveals distinct patterns of myocardial substrate use in humans with coronary artery disease or left ventricular dysfunction during surgical ischemia/reperfusion. *Circulation* **119**, 1736-46.

van Horssen, J., van Schaik, P. and Witte, M. (2017). Inflammation and mitochondrial dysfunction: A vicious circle in neurodegenerative disorders? *Neurosci Lett*.

Vastrik, I., D'Eustachio, P., Schmidt, E., Joshi-Tope, G., Gopinath, G., Croft, D., de Bono, B., Gillespie, M., Jassal, B., Lewis, S. et al. (2007). Reactome: a knowledge base of biologic pathways and processes. *Genome Biol* **8**, R39.

Walsh, D. and Mohr, I. (2011). Viral subversion of the host protein synthesis machinery. *Nat Rev Microbiol* **9**, 860-75.

Wathelet, M. G., Lin, C. H., Parekh, B. S., Ronco, L. V., Howley, P. M. and Maniatis, T. (1998). Virus infection induces the assembly of coordinately activated transcription factors on the IFN-beta enhancer in vivo. *Mol Cell* **1**, 507-18.

Wrobel, L., Topf, U., Bragoszewski, P., Wiese, S., Sztolsztener, M. E., Oeljeklaus, S., Varabyova, A., Lirski, M., Chroscicki, P., Mroczek, S. et al. (2015). Mistargeted mitochondrial proteins activate a proteostatic response in the cytosol. *Nature* **524**, 485-8.

Wu, D., Ren, Z., Pae, M., Guo, W., Cui, X., Merrill, A. H. and Meydani, S. N. (2007). Aging up-regulates expression of inflammatory mediators in mouse adipose tissue. *J Immunol* **179**, 4829-39.

Wu, L. E., Gomes, A. P. and Sinclair, D. A. (2014). Geroncogenesis: metabolic changes during aging as a driver of tumorigenesis. *Cancer Cell* **25**, 12-9.

Xie, X., Lu, J., Kulbokas, E. J., Golub, T. R., Mootha, V., Lindblad-Toh, K., Lander, E. S. and Kellis, M. (2005). Systematic discovery of regulatory motifs in human promoters and 3' UTRs by comparison of several mammals. *Nature* **434**, 338-45.

Zhang, Q., Raoof, M., Chen, Y., Sumi, Y., Sursal, T., Junger, W., Brohi, K., Itagaki, K. and Hauser, C. J. (2010). Circulating mitochondrial DAMPs cause inflammatory responses to injury. *Nature* **464**, 104-7.

Zid, B. M., Rogers, A. N., Katewa, S. D., Vargas, M. A., Kolipinski, M. C., Lu, T. A., Benzer, S. and Kapahi, P. (2009). 4E-BP extends lifespan upon dietary restriction by enhancing mitochondrial activity in Drosophila. *Cell* **139**, 149-60.

Figures

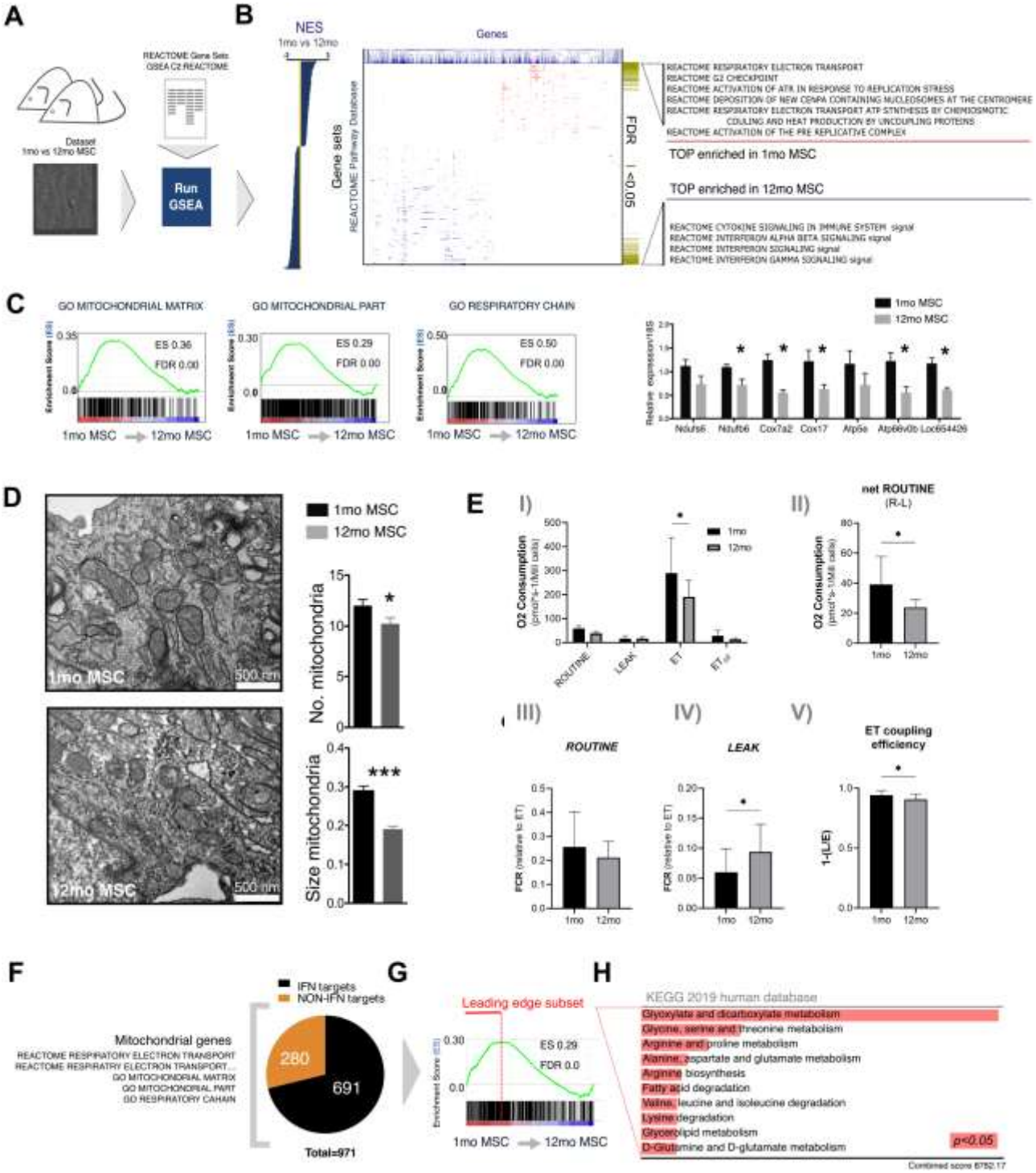

Fig 1. Aging induces increased interferon signaling and diminished mitochondrial gene expression. Microarray dataset of MSC from differently aged (n=3 per group) mice underwent gene set enrichment analysis (GSEA) with a pre-compiled collection of 480 gene

sets from the REACTOME functional category database (A). Gene sets were ranked according to their normalized enrichment score (NES) values (1-month-old MSCs vs 12-month-old MSCs), which account for differences in gene set size and in correlations between gene sets and the expression dataset. The most enriched gene sets in 1-month-old MSCs were related to mitochondrial genes and DNA repair mechanisms, while the most enriched in 12-month-old MSCs were related to the interferon signaling pathway (B). GSEA using gene sets from the Gene Ontology (GO) database confirmed the massive enrichment of different categories of mitochondrial genes in 1-month-old MSCs compared to 12-month-old MSCs (C). qPCR analysis using more biological replicates (n = 6 per group) confirmed the up-regulation of selected mitochondrial genes in 1-month-old MSCs (C,

right panels). Mitochondria were less abundant and were reduced in size in 12-month-old compared to 1-month-old MSCs (unpaired t-test, *p < 0.05 **p < 0.01 ***p < 0.001) (D). Oxidative function is impaired in 12month-old MSC in terms of uncoupled maximal capacity (E,I and II), Flux Control Raios (FCR) (E, III-IV) and ET coupling efficiency (E, V).The mitochondria-related gene sets comprised 971 unique annotated transcripts. Amongst them, 691 were identified as ISGs, according to the INTERFEROME database (F). These 691 genes were significantly enriched in 1mo vs 12mo MSC (G). Leading edge analysis identified 221 genes that contributed the most to the ES. These genes were ontologically related with biochemical pathways of amino acid biosynthesis (H).

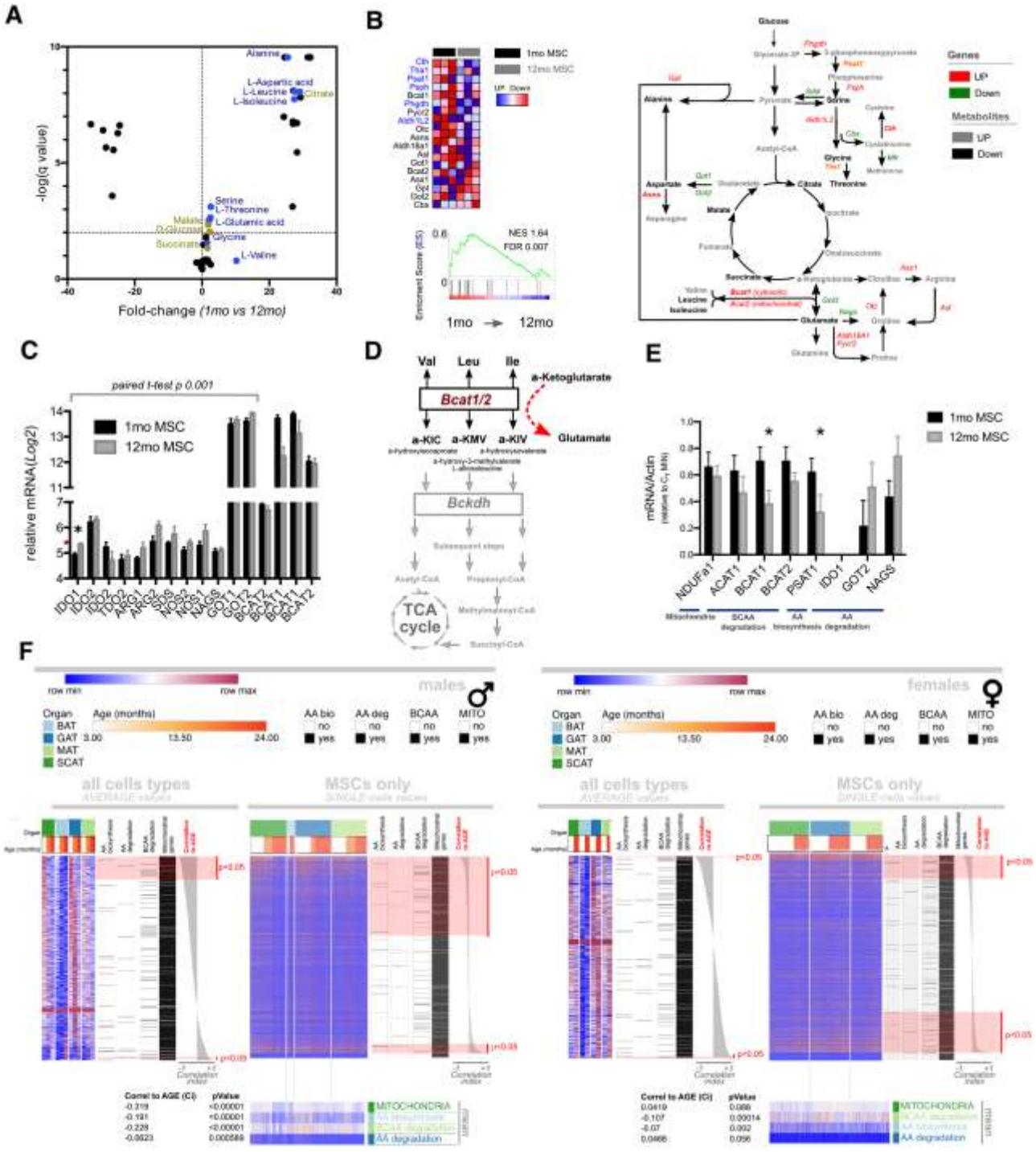

Figure 2. Aging suppresses amino acid biogenesis. Gas chromatography—time of flight mass spectrometry (GC-TOF/MS) revealed many differences in the metabolomic profiles of 1-month-old and 12-month-old MSCs (n=3 per group). The list of metabolites increased with age, included many amino acids (A). Gene set enrichment analysis (GSEA) showed a

significant enrichment of genes encoding for key enzymes of amino acid biosynthesis in 1-month-old vs 12-month-old MSCs (B), especially those involved in the serine and glycine biosynthesis (B, left panel, blue). Most of these genes were either significantly (B, right panel, red bold) or not-significantly (B, right panel, red normal) up-regulated in 1-month-old MSCs, while only 5 out 16 were (not-significantly) down-regulated (B, right panel, green). Genes encoding for the enzymes that catalyzes amino acid degradation were slightly, but coordinately, upregulated in 12-month-old MSCs (C), with the exception are BCAT1 and 2, which catalyze the first reversible step of branched chain amino acid (Val, Leu and Ile) (BCAA) degradation (D). qPCR analysis on a larger number of biological replicates (1mo MSC n=8; 12mo MSC=6) confirmed the down-regulation of mitochondria-, AA biosynthesis- and BCAA degradation-related representative gene and the concomitant up-regulation of representative AA degradation-related genes (E). Analogous changes in the transcriptional profile of mitochondria, AA biosynthesis and BCAA degradation related genes with age were confirmed in males by the analysis of a publicly available repository of single-cell transciptomic data (F). Specifically these gene sets were found significnalty anti-correlated with age in all cell types (as average) and single MSC from different depots of adipose tissue of differently aged mice. Details are provided in the text (unpaired and paired t-test, *$p < 0.05$ **$p < 0.01$ ***$p < 0.001$).

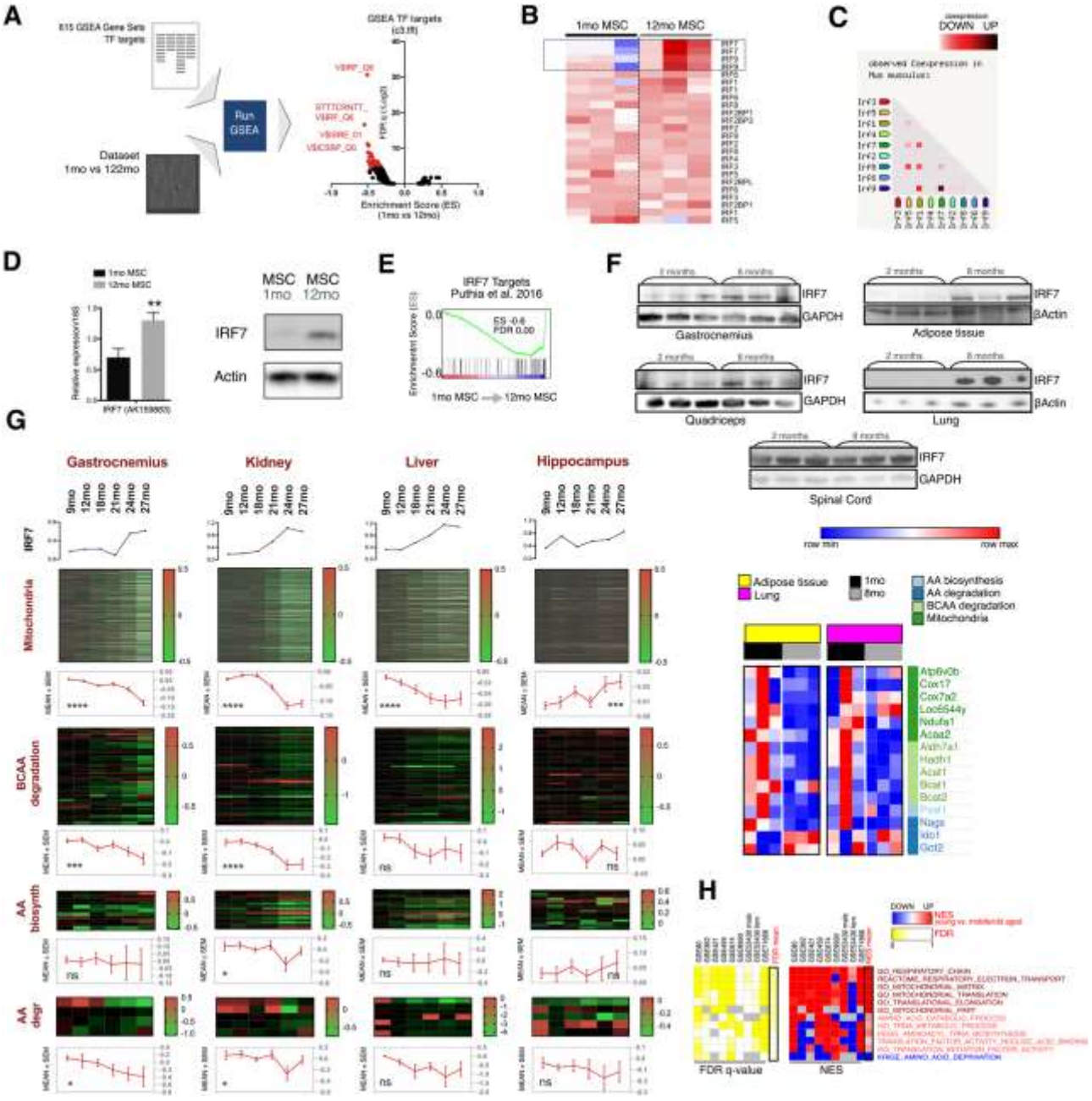

Figure 3. IRF7 increases with aging. Using the GSEA algorithm we interrogated the transcriptomic profiles of 1-month-old (n=3) and 12-month-old MSC (n=3) samples for the enrichment of a precompiled collection of 615 gene sets of transcription factor motifs based on the work of Xie et al(Xie et al., 2005). Genes upregulated in 12-month-old vs 1-month-old MSC were enriched in motifs related to the interferon regulatory factor (IRF) family of transcription factors (A). Among the nine members of this family, IRF7 and, to a much lesser

extent, IRF9, were the only ones whose transcripts were readily up-regulated in 12-month-old compared to 1-month-old MSCs (B). STRING analysis revealed that IRF7 and IRF9 are frequently co-regulated (C). 12-month-old MSCs exhibited increased levels of IRF7 expression with respect to both transcript and protein abundance (D), which was consistent with a significantly elevated level of the transcriptional expression of genes previously identified as IRF7 targets (E). IRF7 protein levels were elevated in multiple organs (gastrocnemius, quadriceps, adipose tissue, lungs), but not in spinal cord, of 8-month-old mice (n=3) compared to 1-month-old mice (n=3). (F, upper panles). IRF7 increase with age in adipose tissue and lung samples was concomitant with diminished expression of mitochondria-, AA biosynthesis- and BCAA degradation-related genes, while AA degradation-related genes resulted up-regulated (adipose tissue) or unchanged (lungs) (F, lower panel). The analysis of a recently published resource of RNA-seq data on varied organs of differently aged rats reveals that the increased upregulation of IRF7 with age is closely correlated with diminished mitochondria-, AA biosynthesis- and BCAA degradation-related genes in gastrocnemious, kidney and liver, but not in hippocampus (G). GSEA analysis revealed the reduced expression of mitochondrial/translation-related genes and increased expression of amino acid deprivation-related genes with age in multiple organs/tissues of multiple species (H). (unpaired t-test, *p < 0.05 **p < 0.01 ***p < 0.001; **panel G**: ANOVA test for linear trend *p < 0.05 **p < 0.01 ***p < 0.001 ****p<0.0001).

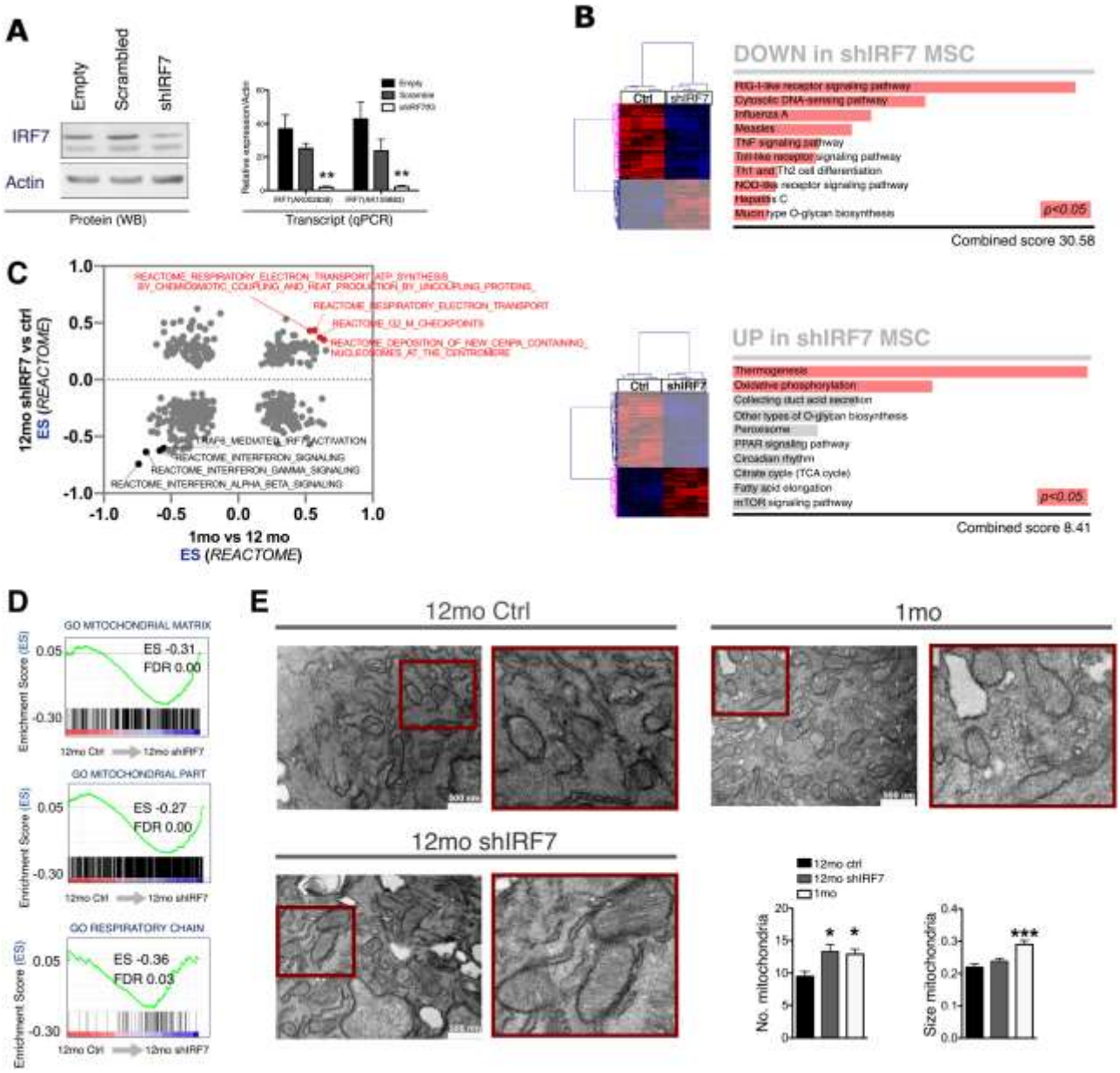

Figure 4. IRF7 silencing reverts mitochondrial gene expression and function. IRF7 was knocked down in 12-month-old MSCs and transcriptional changes were assessed trhough a whole-genome microarray analysis (n=4 per group) (A). Genes with significanlty different expression (t-test, $p < 0.05$) in 12-month-old shIRF7 vs 12-month-old Ctrl MSC were functionally categorized based on the KEGG 2019 mouse algorithm (B). ES values of the REACTOME gene sets between “12-month-old control vs. 12-month-old shIRF7” microarray dataset were calculated through GSEA and plotted vs the corresponding ES

values between “1-month-old vs. 12-month-old” (C). GSEA analysis for three distinct mitochondria-related gene sets from the Gene Ontology Consortium Database confirmed the enrichment of mitochondrial genes in 12-month-old shIRF7 MSCs compared to controls (D). Mitochondria in shIRF7 were significantly more abundant and displayed more structured cristae (One-way ANOVA, Dunett post-hoc *p < 0.05 **p < 0.01 ***p < 0.0001) compared to 12-month-old controls (E).

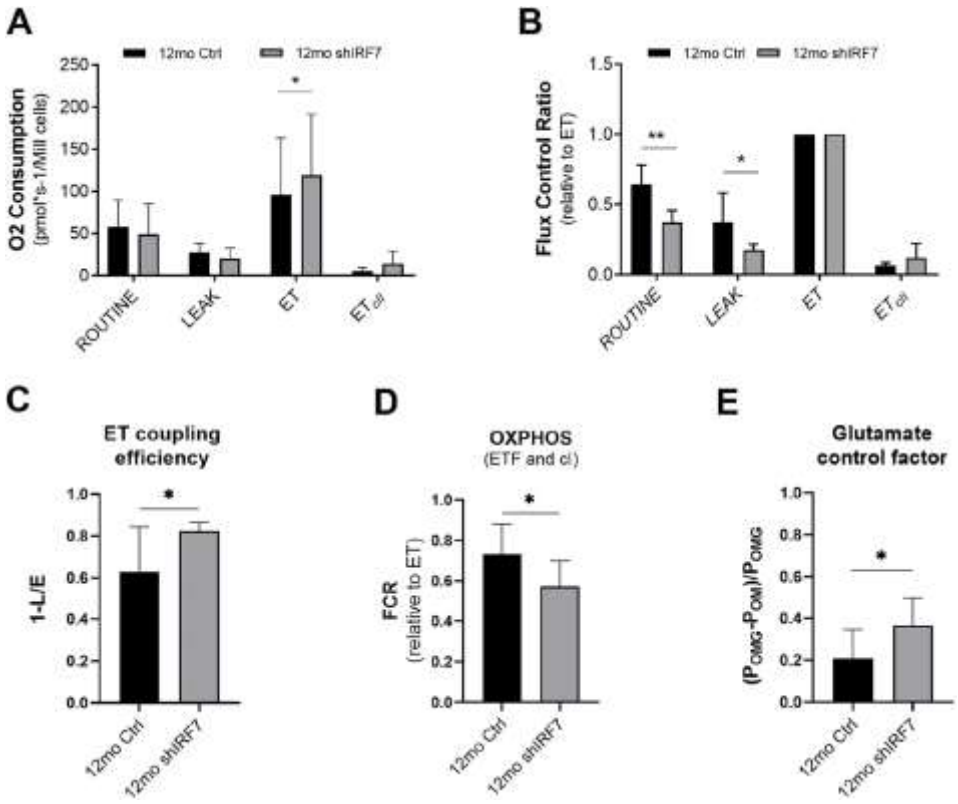

Figure 5. Mitochondrial function was evaluated with high resolution respirometry in 12mo Ctrl or 12mo IRF7 cells. Quantitative analysis of the rates of oxygen consumption in the ROUTINE, LEAK, and ET respiratory states in intact 12mo Ctrl (black) or 12mo IRF7 (grey) cells (A). Qualitative analysis of data of mitochondrial function in intact cells expressed relatively to ET (Flux Control Ratio - FCR) in the respiratory states analyzed (ROUTINE, LEAK and ET) (B). ET coupling efficiency was expressed as 1-(L/E) (C). Flux control ratios (FCR) in the ADP-stimulated OXPHOS state sustained by ETF and complex I (POM) in 12mo Ctrl or 12mo IRF7 permeabilized cells (D). Effect of addition of glutamate in 12mo Ctrl and 12mo IRF7 permeabilized cells evaluated using the control factor POMG-POM/POMG (E). Data are reported as mean±SD, n=5; Two-way ANOVA with Sidak's post-hoc correction (A, B) and paired t-Test (C, D, E); $P<0.05$.

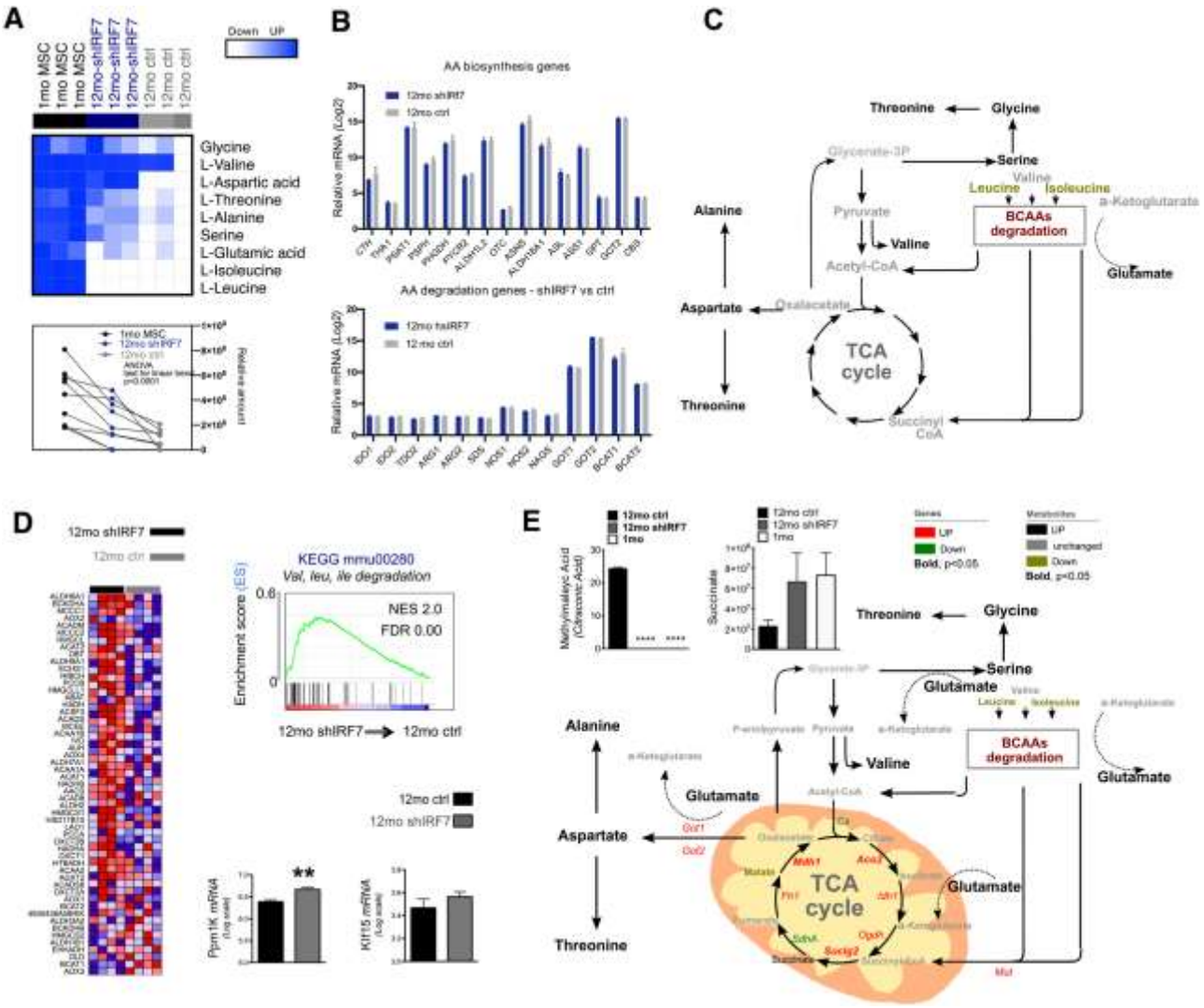

Figure 6. IRF7 knock-down partially restores of the intracellular the amino acid pool. All amino acids reduced in middle aged cells were restored upon IRF7 knock-down, except leucine and isoleucine (A). Genes encoding for the enzyme involved in either amino acid biosynthesis or degradation were not coordinately changed upon Irf7 knockdown (B). BCAA degradation provides glutamate and feeds into TCA cycle, which serves as common precursor of aspartate, alanine, serine and glycine (C). Genes involved in BCAA degradation pathways and their major regulators (such as Ppm1k and Klf15) were enriched upon IRF7 knockdown (D). Genes encoding for the enzyme which catalyzes the various steps of the TCA cycle are significantly upregulated (red bold), non-significantly upregulated (red) or

non-significantly down-regulated (green). Metabolomic and transcriptional profile suggest a model in which BCAA degradation feeds TCA cycle to sustain AA biogenesis (E). (unpaired t-test, *p < 0.05 **p < 0.01 ***p < 0.001).

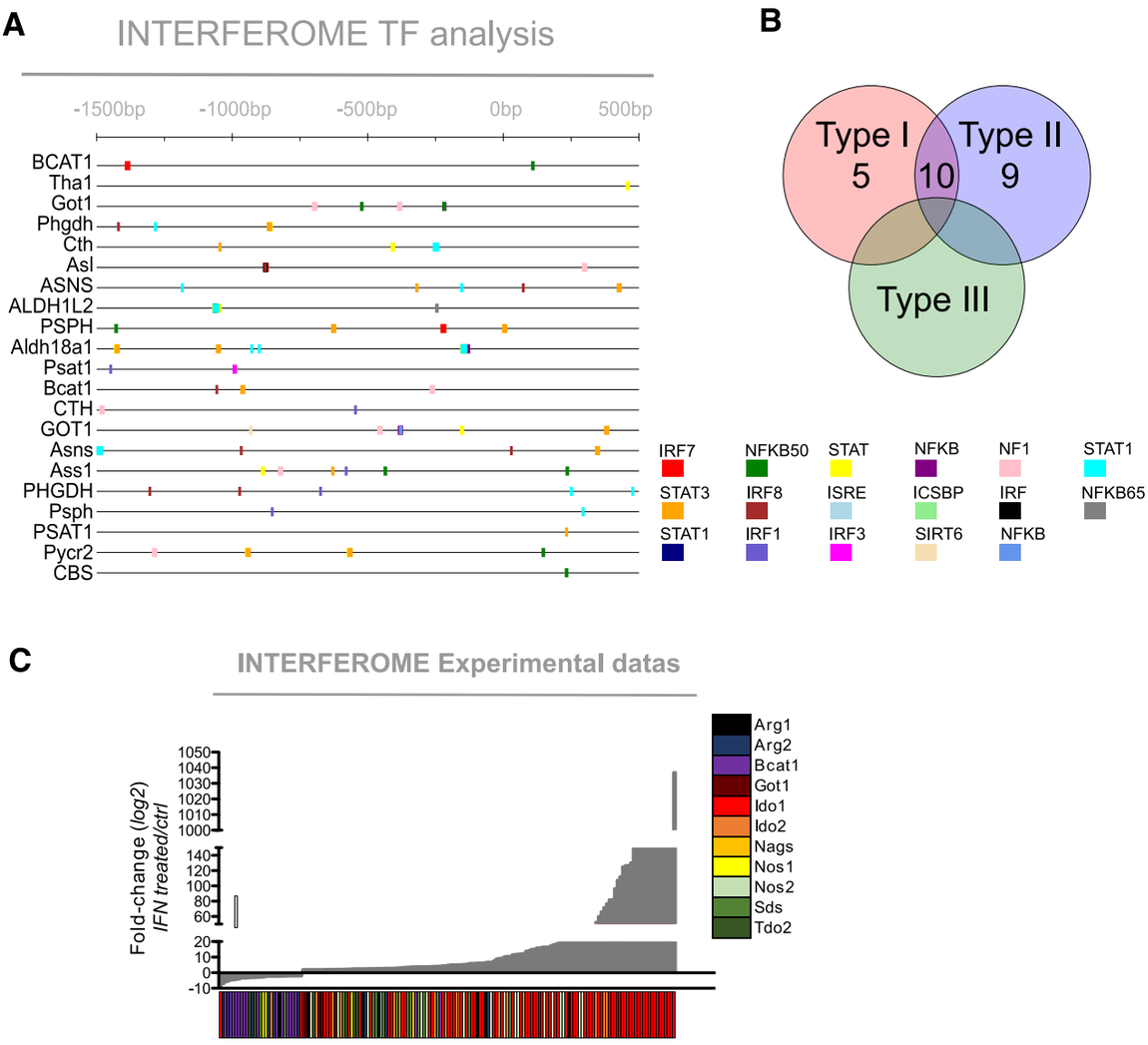

Figure S1. AA biosynthetic genes are ISGs. INTERFEROME database identified the AA biosynthesis genes as interferon stimulated genes (ISGs), on the basis of experimental data in literature which reported changes in their expression (2-fold or greater) upon IFN treatment. INTERFEROME analysis identified IFN-related transcription factor motifs within a sequence spanning from 1500 bp upstream to 500bp downstream the transcriptional start site of these genes (A). Specifically, promoter analysis of these genes reveal that they are potential targets of Type I and Type II IFN (B). Results of experimental data comprised Iin the NTERFEROME Experimental database repository indicate that the AA degradation genes listed in Fig 2C are all IFN target as their expresion change upon IFN treatment. specifically, most of them increase while a few (including Bcat1) is diminisched upon IFN administration (C).

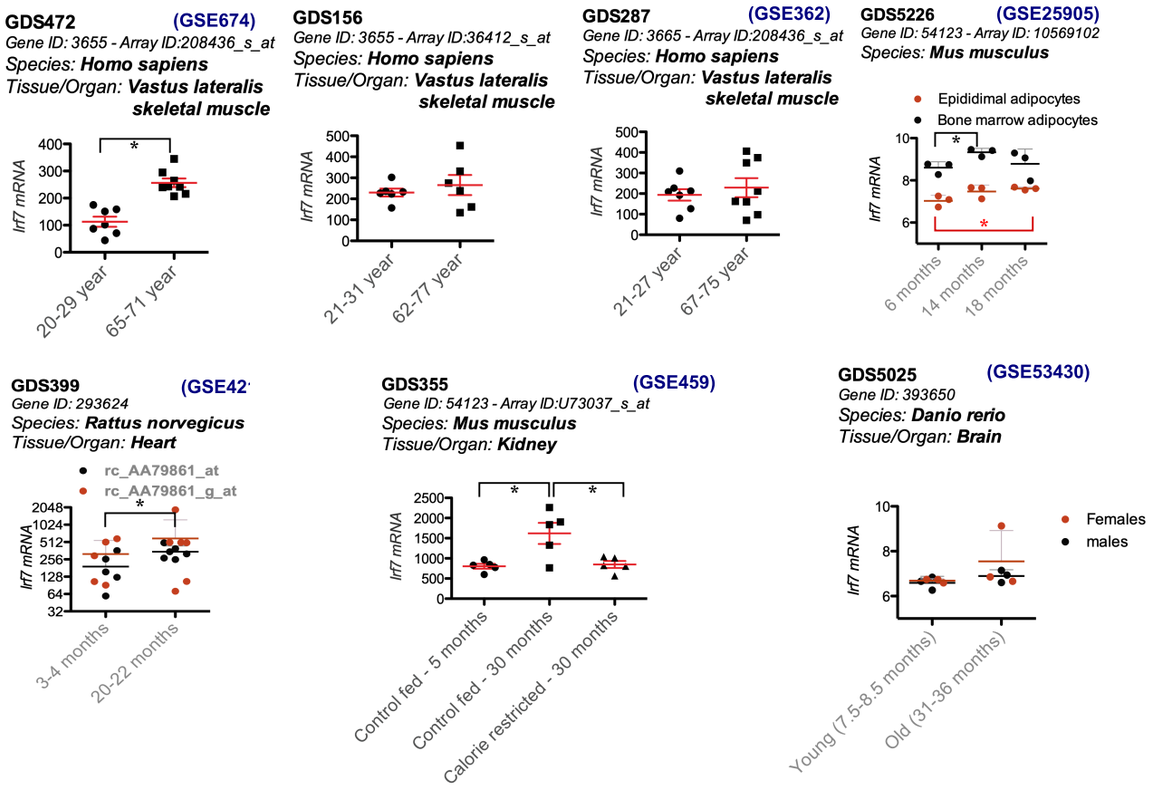

Figure S2. IRF7 is upregulated with age in multiple tissue across different species.

(unpaired t-test or ANOVA with Turkey post-hoc, *p < 0.05 **p < 0.01 ***p < 0.0001).

A

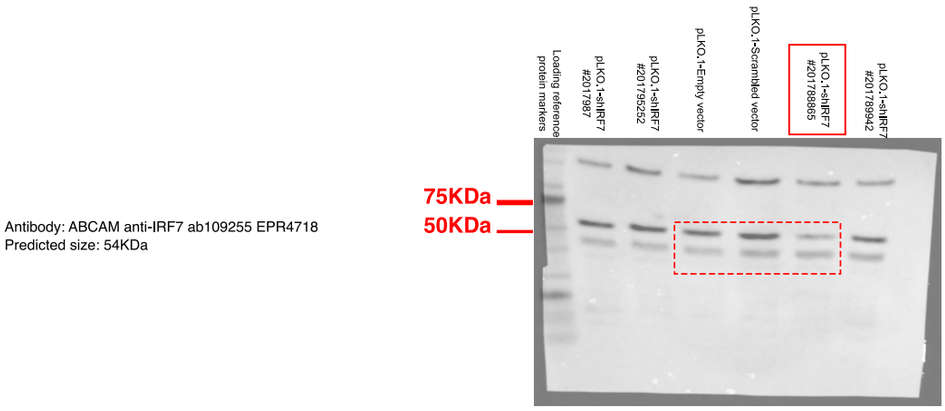
Loading reference protein markers
pLKO.1-shIRF7 #2017987
pLKO.1-shIRF7 #2017935252
pLKO.1-Empty vector
pLKO.1-Scrambled vector
pLKO.1-shIRF7 #2017988985
pLKO.1-shIRF7 #2017989942
75KDa
50KDa
Antibody: ABCAM anti-IRF7 ab109255 EPR4718
Predicted size: 54KDa

B

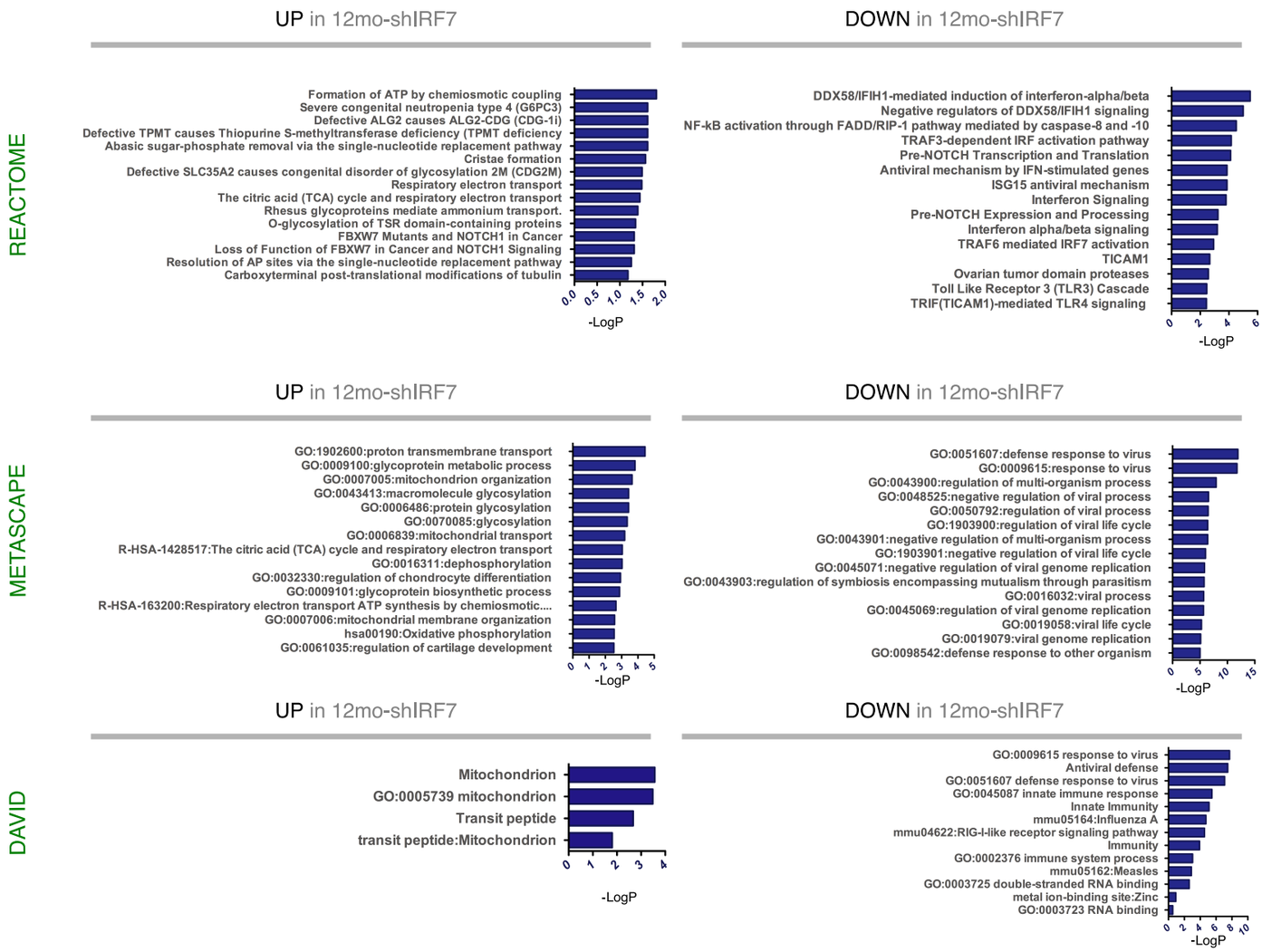
REACTOME
UP in 12mo-shIRF7
Formation of ATP by chemiosmotic coupling
Severe congenital neutropenia type 4 (G6PC3)
Defective ALG2 causes ALG2-CDG (CDG-1i)
Defective TPMT causes Thiopurine S-methyltransferase deficiency (TPMT deficiency
Abasic sugar-phosphate removal via the single-nucleotide replacement pathway
Cristae formation
Defective SLC35A2 causes congenital disorder of glycosylation 2M (CDG2M)
Respiratory electron transport
The citric acid (TCA) cycle and respiratory electron transport
Rhesus glycoproteins mediate ammonium transport.
O-glycosylation of TSR domain-containing proteins
FBXW7 Mutants and NOTCH1 in Cancer
Loss of Function of FBXW7 in Cancer and NOTCH1 Signaling
Resolution of AP sites via the single-nucleotide replacement pathway
Carboxyterminal post-translational modifications of tubulin
0.0 0.5 1.0 1.5 2.0
-LogP
DOWN in 12mo-shIRF7
DDX58/IFIH1-mediated induction of interferon-alpha/beta
Negative regulators of DDX58/IFIH1 signaling
NF-kB activation through FADD/RIP-1 pathway mediated by caspase-8 and -10
TRAF3-dependent IRF activation pathway
Pre-NOTCH Transcription and Translation
Antiviral mechanism by IFN-stimulated genes
ISG15 antiviral mechanism
Interferon Signaling
Pre-NOTCH Expression and Processing
Interferon alpha/beta signaling
TRAF6 mediated IRF7 activation
TICAM1
Ovarian tumor domain proteases
Toll Like Receptor 3 (TLR3) Cascade
TRIF(TICAM1)-mediated TLR4 signaling
0 2 4 6
-LogP
METASCAPE
UP in 12mo-shIRF7
GO:1902600:proton transmembrane transport
GO:0009100:glycoprotein metabolic process
GO:0007005:mitochondrion organization
GO:0043413:macromolecule glycosylation
GO:0006486:protein glycosylation
GO:0070085:glycosylation
GO:0006839:mitochondrial transport
R-HSA-1428517:The citric acid (TCA) cycle and respiratory electron transport
GO:0016311:dephosphorylation
GO:0032330:regulation of chondrocyte differentiation
GO:0009101:glycoprotein biosynthetic process
R-HSA-163200:Respiratory electron transport ATP synthesis by chemiosmotic....
GO:0007006:mitochondrial membrane organization
hsa00190:Oxidative phosphorylation
GO:0061035:regulation of cartilage development
0 1 2 3 4 5
-LogP
DOWN in 12mo-shIRF7
GO:0051607:defense response to virus
GO:0009615:response to virus
GO:0043900:regulation of multi-organism process
GO:0048525:negative regulation of viral process
GO:0050792:regulation of viral process
GO:1903900:regulation of viral life cycle
GO:0043901:negative regulation of multi-organism process
GO:1903901:negative regulation of viral life cycle
GO:0045071:negative regulation of viral genome replication
GO:0043903:regulation of symbiosis encompassing mutualism through parasitism
GO:0016032:viral process
GO:0045069:regulation of viral genome replication
GO:0019058:viral life cycle
GO:0019079:viral genome replication
GO:0098542:defense response to other organism
0 5 10 15
-LogP
DAVID
UP in 12mo-shIRF7
Mitochondrion
GO:0005739 mitochondrion
Transit peptide
transit peptide:Mitochondrion
0 1 2 3 4
-LogP
DOWN in 12mo-shIRF7
GO:0009615 response to virus
Antiviral defense
GO:0051607 defense response to virus
GO:0045087 innate immune response
Innate Immunity
mmu05164:Influenza A
mmu04622:RIG-I-like receptor signaling pathway
Immunity
GO:0002376 immune system process
mmu05162:Measles
GO:0003725 double-stranded RNA binding
metal ion-binding site:Zinc
GO:0003723 RNA binding
0 2 4 6 8 10
-LogP

Figure S3. Irf7 knock-down reverts age-induced transcriptional changes. Whole membrane of the western blot of the protein extracts from 12mo MSC infected either with control vectors or different clones of shIRF7 shows the clone #201788865 provides effecient knock-down of IRF7. The dashed red frame indicates the crop reported in Fig 4A (A). Genes significantly ($p < 0.05$) up-regulated and down-regulated upon Irf7 knock-down displayed mitochondria-related functional enrichment and anti-viral response gene enrichment, respectively, according to multiple functional databases (REACTOME, METASCAPE, DAVID) (B).

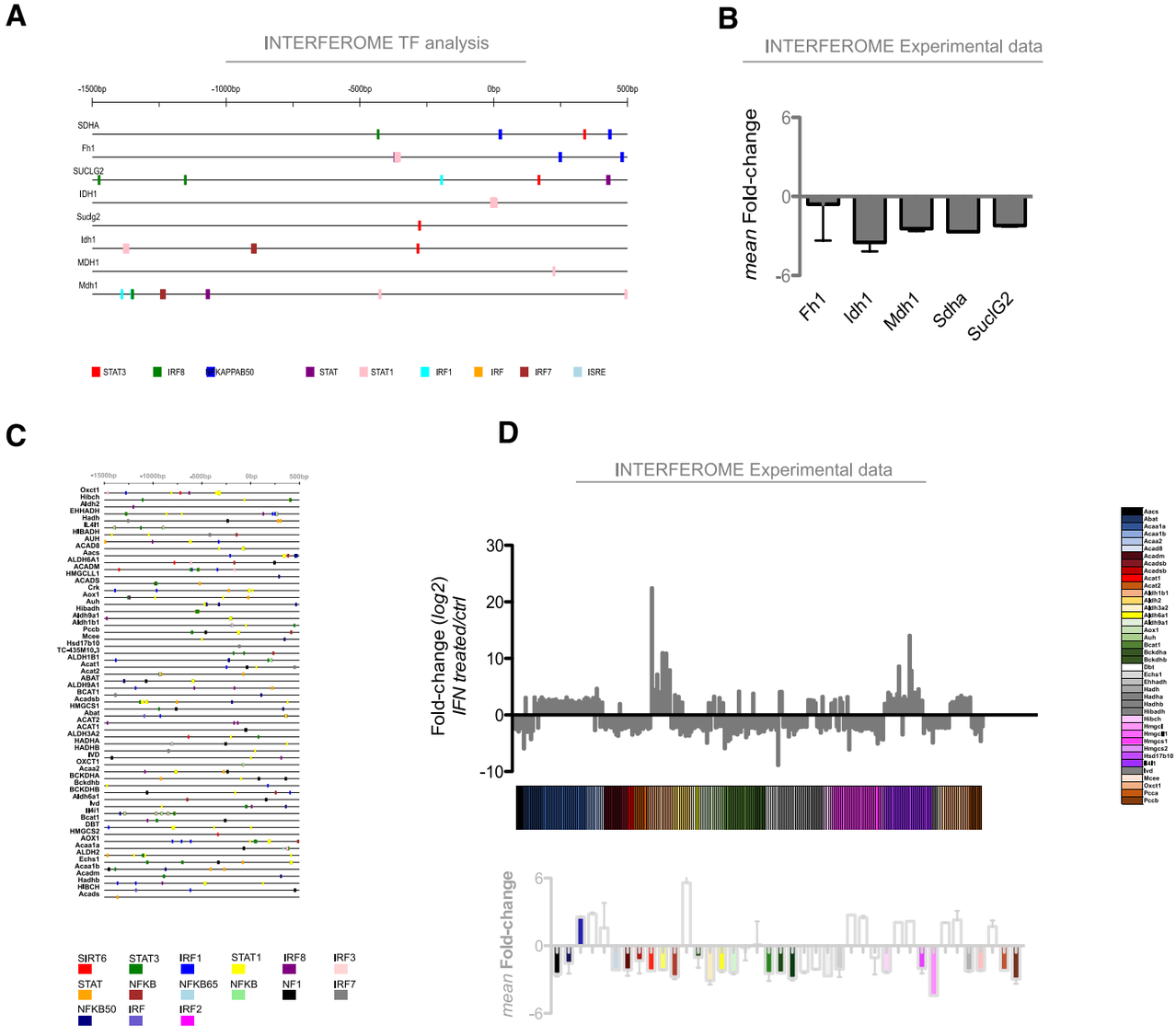

Figure S4. TCA cycle and BCAA degradation genes are ISGs. Genes encoding for the enzymes involved in the TCA cycle reported in Fig 6C were recognized as interferon stimulated genes (ISGs) according to data within the INTERFEROME database and many IFN-related transcription factor motifs were identified within their promoter regions (A). These genes are predicted to be downregulated upon IFN treatment according to INTERFEROME experimental data sets (B). Genes encoding for enzymes involved in branched chain amino acid (BCAA) degradation are identified as ISGs according to the INTERFEROME database, display multiple IFN-related transcriptional motifs within their promoter regions (C) and were generally downregulated upon IFN treatment (D).

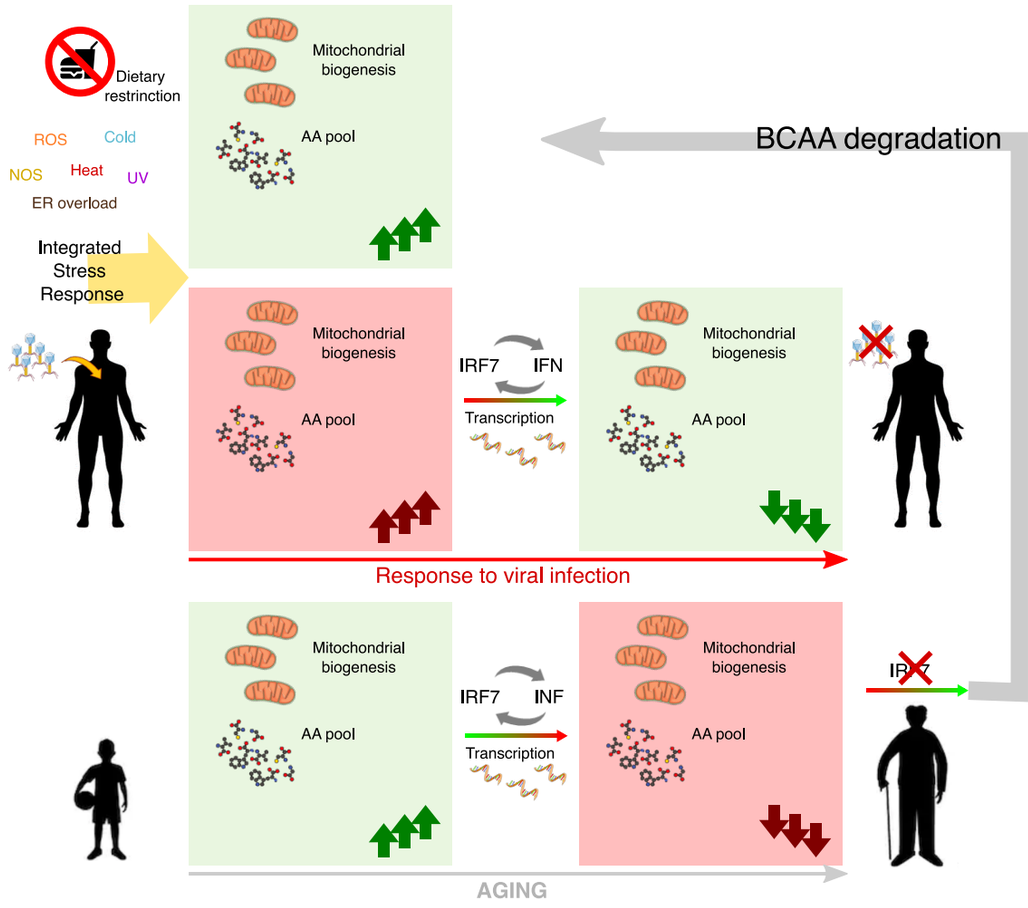

Figure S5. Model showing that aging is mediated by the untimely activation of IRF7-IFN signaling pathway which impairs "core" longevity-related biological functions. Mitochondrial and amino acid biogenesis are the common outcomes of successfully integrating stress response pathways and life-extending interventions such as dietary restriction. Viruses are thought to stimulate integrated stress responses, with the aim of commandeering host bioenergetic and biosynthetic machinery for the replication of viral particles. To prevent this effect, cells have evolved IFN signaling pathways, which shut off these functions. Aging induces the untimely activation of this process (in the absence of a real viral infection) with detrimental effects on organism fitness and longevity. IRF7 inhibition restores mitochondrial biogenesis and rescues the amino acid pool, likely though the activation of BCAA degradation pathways which feed TCA cycle anaplerosis supporting amino acid biosynthetic pathways.

Acc.no.	Gene	Species	Forward	Reverse
NM_010888.1	*Ndufs6*	*mus musculus*	GAACGAGGTGGAGCACCGCA	GCAGGCCGCAGTAGCCACAT
NM_001033305.1	*Ndufb6*	*mus musculus*	AGCAGCTGCGGGAGCTAAGGA	GGCCCCGTCCCGCAAAAAGT
NM_009945.2	*Cox7a2*	*mus musculus*	GCCGTTTCCGGTCTGGTGGCTT	ACGAAGGGCCAGCAGATTCCG
NM_001017429.2	*Cox17*	*mus musculus*	GCGGAAGTGGAGACAGACGGC	CCGCCAGTCCCGGCATCTTT
NM_025983.2	*Atp5e*	*mus musculus*	CCGGGCCGGTTTGAGGCTAC	CCAGCCTGTCGCCAGTACGC
NM_033617.1	*Atp6v0b*	*mus musculus*	GGCCTGTTTGGGGTCATTGTTGC	GCACGGCCCCACCCATACAG
NR_002690.1	*Loc654426*	*mus musculus*	ACATTGGTGTTACAGCTGTGGCCT	GGTCCTCCAGATGCCTGTCGC
BC024364	*Ndufa1*	*mus musculus*	GTCCACTGCGTACATCCACA	ACGTCTATCGCGTTCCATCA
BC024763	*Acat1*	*mus musculus*	GCTGGAGATTGACCCCCAAA	GCTTCAGGGCATGAGCCATA
BC053706	*Bcat1*	*mus musculus*	CTCTCCATCTTCCGCGCTTG	ATTTCTCGTGGCTTGGGTCG
BC017688	*Bcat2*	*mus musculus*	ACCCTTCATTCGTCAGAGCC	CAGCCACAGTGGGTCCATAG
BC005657	*Psat1*	*mus musculus*	TATGTATGCCCAGTGGAGCG	CTTCGTCTCCTTTGGCGTTG
NM_002164.6	*Ido1*	*mus musculus*	ATGCAGACTGTGTCTTGGCA	AGAACAAAACGTCCATGTTCTCAT
BC009812	*Got2*	*mus musculus*	GTGGTCCGCAATGAGTTCAC	CACCTTCCAGCTTGACGACT
BC057990	*Nags*	*mus musculus*	TTTTTGGCGGCGGATCAGTA	TGGATTCCAGACACCACTGC
AK159883	*Irf7*	*mus musculus*	CGGGAGCTTGGATCTACTGTG	CTTGCCAGAAATGATCCTGGG
AK002830	*Irf7*	*mus musculus*	CAGCCACATACTGGAATCCG	CTGCATGCTGCATAGGGTTC
X03765.1	*Actin*	*mus musculus*	CATCGTGGGCCGCTCTA	CACCCACATAGGAGTCCTTCTG
NR_003278.3	*18s*	*mus musculus*	ACCGCAGCTAGGAATAATGGA	GCCTCAGTTCCGAAAACCA

Table 1. List of primers used for qPCR analysis.